

American Journal of Science

JUNE 2011

EVIDENCE FOR OCEANIC CONTROL OF INTERANNUAL CARBON CYCLE FEEDBACKS

JEFFREY PARK

Department of Geology and Geophysics, Yale University, P.O. Box 208109,
New Haven, Connecticut, 06520-8109; Jeffrey.Park@yale.edu

ABSTRACT. Large-scale carbon-cycle feedbacks within Earth's climate system can be inferred from the statistical correlation of atmospheric CO₂ and other climate observations. These statistical relationships can serve as validation targets for global carbon-cycle models. Fourier-transform coherence between atmospheric CO₂ measured at Mauna Loa, Hawaii, and Hadley Centre global-average temperatures changed in the late 20th century at interannual frequencies, from a 6-month time lag to a 90° phase lag that scaled CO₂ fluctuations to a time-integral of the global-average temperature anomaly. Wavelet coherence estimates argue that this change occurred with a recognized ocean-circulation climate transition during the late 1970s. General features of these CO₂-temperature correlations are confirmed using global-average temperature from other sources and atmospheric CO₂ measured at other locations, though only the Mauna Loa CO₂ record is long enough to resolve well the coherence properties before the 1970s transition. The CO₂-coherence phase for the global-average surface-air temperature time series from NASA-GISS and the lower-troposphere temperature series from the MSU satellite is more complex than for the Hadley-Centre dataset, the only estimate that incorporates sea-surface temperature (SST) observations. Near $f = 0.25$ cyc/year, 4-year oscillation period, the CO₂-coherence is particularly strong for the Hadley-Centre gridpoint temperature-anomaly time series from low-latitude oceans. This suggests that sea-surface temperature is a primary driver of the correlation, at least for the $0.2 < f < 0.5$ cyc/yr bandpass where the El-Nino/Southern-Oscillation (ENSO) climate process dominates. Outside the ENSO bandpass coherence is significant between 14 long-running GLOBALVIEW CO₂-observing sites and the sea-level-pressure-based Southern Oscillation Index (SOI) and North Atlantic Oscillation (NAO) time series, consistent with wind stress and mixed-layer-thickness influences on ocean-atmosphere CO₂ flux, independent of temperature fluctuations. Evidence for terrestrial biosphere influence is strongest in the leading principal component of GLOBALVIEW CO₂-variability at $f = 0.25$ cpy, where a larger amplitude and a 4-month phase shift distinguish the mid- and high-latitude Northern Hemisphere CO₂ fluctuations from those of the tropics and the Southern Hemisphere. The terrestrial signal we infer, however, coheres more strongly with oceanic-gridpoint temperatures than to continental-gridpoint temperatures.

Key words: Carbon cycle, greenhouse feedbacks, ocean circulation, climate change, El-Nino/Southern-Oscillation (ENSO), North Atlantic Oscillation (NAO) and interannual temperature fluctuations

INTRODUCTION

Carbon-cycle feedbacks influence the absorption of anthropogenic CO₂ by the Earth system. Understanding these feedbacks is key for monitoring and perhaps enhancing net carbon sequestration in the future. Uncertainties in carbon-cycle models remain large, so it can be useful to examine correlations between climate and carbon-cycle time series, independent of computer-simulation models. Data correla-

tions do not imply causality, but they can be used to support or undermine causal hypotheses, and to suggest new hypotheses. The explosive growth in CO₂ data collection encourages the intensive analysis of transient climate events (for example, Chavez and others, 1999), but Earth's climate system contains processes that operate on a range of time scales. It is therefore pertinent to estimate correlation and coherence across different frequencies with the tools of spectrum analysis, to complement and contrast time-domain correlations. Many familiar causal relationships embedded within stochastic signals can be expressed via simple models of coherence and correlation amplitude and phase in the frequency domain. For illustrative examples with open-source software, see the online supplement of Park (2009).

Given the complexities of Earth's carbon cycle, it is perhaps surprising that atmospheric CO₂ observations correlate significantly with global-average properties of Earth's meteorology. Nevertheless, Kuo and others (1990) found strong spectral coherence between 1958 to 1988 global-average temperature fluctuations ΔT_i and interannual CO₂ variability measured at Mauna Loa, Hawaii, the longest CO₂ time series with monthly sampling (Keeling, 2008). Revisiting the problem 20 years later, Park (2009) found a subtle, but significant, transition in the correlation. Starting from a fixed 6-month time lag during 1958 to 1988, similar to that reported by Kuo and others (1990), during 1979 to 2008 a constant 90° phase lag across frequencies $0.2 < f < 0.7$ cyc/yr related CO₂ roughly to a simple integral of temperature fluctuations. Was this transition caused by (1) the gradual saturation of the oceanic sink for atmospheric CO₂ (Le Quere and others, 2007; Schuster and others, 2009; Khatiwala and others, 2009); (2) an abrupt transition of the ocean circulation (Trenberth, 1990; Graham, 1994; Park and Mann, 2000; Meehl and others, 2009); or (3) a statistical artifact related to a particular CO₂ observation site and a particular global-average temperature time series? This study argues for option (2), and also explores additional relationships among climate and carbon-cycle processes.

In this paper, we examine correlations among a set of earth-system data series, principally with Fourier and wavelet-based spectrum analysis, to relate interannual CO₂-temperature coherence to carbon-cycle processes in the last half-century. We find that interannual ocean-climate fluctuations typically have the simplest coherence relationships with CO₂, which validates the notion that they are the primary driver of interannual CO₂ fluctuations. Land regions either exert secondary CO₂ feedbacks or operate in close linkage with ocean-climate fluctuations. The Background section reviews past work on interannual correlations between climate and atmospheric CO₂ data. Here we note that 1990s studies confirmed the Kuo and others (1990) coherence between CO₂ and temperatures, suggesting a linkage via oceanic CO₂ exchange, but were followed after 2000 by many inverse studies of CO₂ variability that neglected oceanic processes in favor of terrestrial-biosphere influence. The Data section discusses the data time series used in this study. Fourteen globally distributed 30-year CO₂ time series are available, matched by global-average temperature time series from satellite measurements, from meteorological stations, and from a mix of meteorological stations and shipboard sea-surface temperature measurements. The Methods section reviews spectrum-analysis methods, based on multiple-taper spectrum analysis and a related multiple-wavelet algorithm, to correlate pairs of time series with coherence estimates, or multiple records with a spectral-domain singular-value decomposition (SVD). The section titled *The Coherence Between Atmospheric CO₂ and Global Temperature* compares CO₂-coherence with global-temperature time series from competing sources, expanding the restricted focus of Park (2009). Although global-average temperature times series from multiple sources show significant coherence with atmospheric CO₂, the amplitude and phase relationships with the time series provided by the Climate Research Unit at the University of East Anglia lead to the

simplest time-domain interpretation. The section titled *When and How Did the Shift in Coherence Phase Occur?* uses wavelet spectra and coherence to elucidate the coherence transition reported by Park (2009), linking it temporally to the reported ocean-circulation shift in the late 1970s in the northern Pacific. The section titled *The Coherence Between Atmospheric CO₂, NAO and SOI* addresses CO₂-coherence with the Southern Oscillation Index (SOI) and North Atlantic Oscillation (NAO). We detect CO₂-coherence with distinct phase lags for SOI inside and outside the El-Nino/Southern-Oscillation (ENSO) passband, and detect correlation between NAO and the global carbon cycle at decadal time scales. The Discussion section discusses the results. The Appendix further examines the spatial variability of CO₂ fluctuations on ENSO time scales, illustrating the strong coherence of CO₂ measurements worldwide with tropical SST fluctuations.

BACKGROUND

At interannual time scales, CO₂ fluctuations lag behind global-temperature fluctuations (Kuo and others, 1990; Martin and others, 1994; Dettinger and Ghil, 1998; Adams and Piovesan, 2005; Park, 2009). Causative carbon-cycle feedback processes potentially include the response of the terrestrial biosphere to local temperature fluctuations, drought and fire (Buermann and others, 2007; Field and others, 2009; Zhao and Running, 2010), sea-surface temperatures, wind stress and ocean circulation (Chavez and others, 1999; Obata and Kitamura, 2003; Takahashi and others, 2009; Gruber and others, 2009), silicate weathering (Stallard, 1998; Gaillardet and others, 1999; Hilley and Porder, 2008; Raymond and others, 2008), volcanic eruptions (Lucht and others, 2002; Reichenau and Esser, 2003; Gu and others, 2003), and organic-carbon transport and burial in terrestrial watersheds (Stallard, 1998; Gudacz and others, 2010). Even with the advent of a global network of CO₂-monitoring stations (Masarie and Tans, 1995; GLOBALVIEW-CO₂, 2009), and the inspiring data-fits and visualization tools of modern data-assimilation models (Peters and others, 2007), the multiplicity of contributing factors formally makes the inverse-modeling of CO₂ variability an ill-posed problem (for example, Parker, 1994, Chapter 2).

The land biosphere and the ocean are estimated to sequester comparable quantities of anthropogenic carbon, 1.5 to 2 GtC/yr each (Lee and others, 1998; Battle and others, 2000; Canadell and others, 2007; Houghton, 2007). Although carbon-cycle models focused on oceanic exchanges have been applied to interannual CO₂ variability (for example, McKinley and others, 2006), several interpretations of interannual CO₂ fluctuations have focused on land-biosphere response and neglect oceanic responses (Lee and others, 1998; Bousquet and others, 2000; Russell and Wallace, 2004; Zeng and others, 2005; Buermann and others, 2007; Qian and others, 2008). One possible justification for the narrow focus is that the large annual cycle in CO₂ time series is dominated by the seasonal cycle of terrestrial plant growth (Peters and others, 2007). Another justification is the prediction of weak interannual variability in the net oceanic CO₂ uptake in some carbon-cycle models, for example Lee and others (1998). However, carbon-cycle models do not all predict a near-constant oceanic CO₂ uptake (for example, Rodenback and others, 2003; Raynaud and others, 2006; Park and others, 2006), and attempts by Butler and others (2007) to fit CO₂ variability in the vegetation-poor boreal Southern Hemisphere led them to conclude that oceanic CO₂ flux was crucial. Boyce and others (2010) reported correlation between ENSO and historical phytoplankton abundance that suggests additional oceanic processes at work. The recent shift in the annual CO₂ cycle (Piao and others, 2008) suggests that enhanced CO₂-uptake by the terrestrial biosphere may largely be cancelled by CO₂ respiration from enhanced plant decay, reducing the contribution of terrestrial "greening" to interannual variability. Moreover, interannual CO₂ fluctuations in the terrestrial biosphere are linked more closely with oceanic ENSO variability than other

factors (Nagai and others, 2007; Qian and others, 2008; Cadule and others, 2010). Ice-cover considerations (Olsen and others, 2003) and shipboard measurements (Watson and others, 2009) suggest that the important North Atlantic locus of CO₂-uptake varies year-to-year by 50 percent or more.

Attempts to verify temperature-CO₂ coherence in environmental time series have highlighted linkages via the tropical ocean. Interannual CO₂-variations were associated with ENSO using spectral coherence (Martin and others, 1994), lagged cross-correlation (Dettinger and Ghil, 1998), empirical-orthogonal-function (EOF) decomposition (Lintner, 2002), and other time-domain methods. Using the 5° × 5° Had-Crut3 gridded temperature times series (Brohan and others, 2006), Park (2009) found strong spectral coherence between interannual sea-surface temperature (SST) fluctuations and CO₂-fluctuations at three widely-spaced locations (Mauna Loa, Hawaii; Barrow, Alaska; South Pole). Appendix A shows additional examples. Weak spectral coherence was found with continental temperature fluctuations. These results appear at variance with the principal causative hypotheses for interannual CO₂ fluctuations considered by many global carbon-cycle modeling studies (Lee and others, 1998; Bousquet and others, 2000; Russell and Wallace, 2004; Zeng and others, 2005; Buermann and others, 2007; Qian and others, 2008). The actual disagreement may be less drastic, because other climate processes are correlated with tropical SST via ENSO.

Transition from a simple time lag to a quadrature relationship may explain why recent estimates of time-domain correlation between CO₂ and SST fluctuations have failed to find a link, for example, Adams and Piovesan (2005). A broadband 90° phase relationship between two time series is best detected with frequency-domain correlation, rather than time-domain correlation. Moreover, simple models for surface-ocean pCO₂ and CO₂-exchange at the sea surface (Nevison and others, 2008; Takahashi and others, 2009; Gruber and others, 2009) imply that tropical SST fluctuations should affect the time-derivative of atmospheric CO₂, consistent with the 90° interannual coherence phase since 1979 reported by Park (2009)—see also Butler and others (2007). Less gas can be dissolved in warmer surface waters, so the rate of CO₂ uptake by the ocean, that is, its time derivative, should correlate directly with SST. A similar correlation with the time-derivative of atmospheric CO₂ would be expected if tropical SST fluctuations caused simultaneous fluctuations in sea-surface wind stress, phytoplankton abundance, cyclic removal of sea-ice, or other processes that influence the atmosphere ocean CO₂ flux. Possible relationships with the land biosphere are likely to interact with the seasonal cycle of plant growth, so a direct correlation between temperature and CO₂ flux cannot be posited with the same confidence. Nevertheless, we find clear support for terrestrial biosphere influence in the ENSO passband, but with timing linked to SST via ENSO teleconnections. Outside the ENSO bandpass, we find simpler correlations with the climate indices based on sea-level pressure differences (SOI, NAO) than with temperatures, as discussed in the Coherence Between Atmospheric CO₂, NAO and SOI section.

DATA

We obtained monthly data for atmospheric CO₂ concentrations at Mauna Loa, Hawaii and the South Pole from the Carbon Dioxide Information Analysis Center (Keeling and others, 2009; <http://cdiac.ornl.gov/trends/co2/>). The Mauna Loa CO₂ time series is continuous from 1958 to present, but serious gaps in South Pole data collection occur before 1965. The GLOBALVIEW data product (GLOBALVIEW-CO₂, 2009; Masarie and Tans, 1995; <http://www.esrl.noaa.gov/gmd/ccgg/GLOBALVIEW/>), provides quasi-weekly CO₂ data (48 samples/yr) for individual stations of a global network, including Mauna Loa (**mlo**) and South Pole (**spo**). GLOBALVIEW-CO₂ offers two multivariate time-series data products for the 1979 to 2008 interval, one in

which the data series at individual observing sites are made gap-free and extended with a global interpolation scheme (EXT data product), and another in which CO₂ at the marine boundary layer (MBL data product) is estimated at a set of 41 latitude values. Although CO₂ measurements at a particular location often exhibit local effects (Thoning and others, 1989), at annual and interannual time scales the observations average over broad regions of both land and ocean. See Appendix A for verification of long-range correlations.

We used temperature data series from contrasting sources. The HadCrut3 global gridded monthly temperature anomaly data set (Brohan and others, 2006) is consolidated to form global- and hemisphere-average monthly temperature-anomaly data sets (<http://www.cru.uea.ac.uk/cru/data/>). For the gridded data we interpolated any data gaps of three months or fewer at individual gridpoints. The 1958 to 2008 Mauna Loa data series could be correlated against 1194 gridpoints, and the 1979 to 2008 GLOBALVIEW data series could be correlated against 1316 gridpoints. We restored the mean 1961 to 1990 yearly cycle to the HadCrut3 temperature data to facilitate comparison with the CO₂ time series, which contain the annual cycle. We used GISTEMP temperature data from the NASA Goddard Institute for Space Science (<http://data.giss.nasa.gov/gistemp/>), based on historical data from meteorological stations. The GISTEMP data product provides global, hemispherical and zonal averages since 1850 (Hansen and others, 1999), as well as a code to produce temperature time series at geographical gridpoints. NASA-GISS offers data products both with, and without, the historical SST measurements compiled by the Hadley Centre. We chose the data set that does not include the SST data to decrease overlap with the Hadley-Centre data. There are two sources for lower tropospheric temperature data from the Microwave Sounding Unit (MSU) satellite, the University of Alabama, Huntsville (UAH), National Space Science and Technology Center (<http://www.nsstc.uah.edu/data/msu/>) and Remote Sensing Systems (RSS, <http://www.remss.com>). This satellite data is available only from 1979 (Spencer and Christy, 1990; Mears and others, 2003), but offers vertical averages of Earth's atmosphere for global-, hemispheric-, and gridded time series, with no geographical gaps aside from the extreme polar regions.

Temperature time series from different data sources can be used to test the robustness of conclusions about historical climate change. Each dataset has weaknesses and strengths, and is subject to corrections and adjustments that can alter details of climate history (Brohan and others, 2006; Thompson and others, 2008) and resolve major disagreements over climate trends (Sherwood and others, 2005; Christy and others, 2007; Santer and others, 2008). Some differences between data sets are specious, such as the warmest-year-in-history honor between the HadCrut3 (warmest=1998) and GISTEMP (warmest=2005) data sets, but others reveal substantive interactions within Earth's climate system, as we argue below.

Finally, atmosphere-ocean CO₂-exchange is facilitated both by SST and the thickness of the mixed layer (Takahashi and others, 2002). The North Atlantic Ocean is a significant carbon sink whose mixed-layer thickness increases with surface-wind intensity. Storminess in the North Atlantic and other high-latitude regions may correlate better than local SST with CO₂ fluctuations, and offer further insight into carbon-cycle dynamics. We use a time series of the North Atlantic Oscillation (Hurrell and Deser, 2009) since 1950 available from the NOAA Climate Prediction Center (<http://www.cpc.noaa.gov/>). We also obtained a time series since 1951 of the Southern Oscillation Index from the same NOAA website. Both NAO and SOI time series are based on normalized pressure differences between fixed points on the globe, and are proxies for large-scale atmospheric circulation patterns.

METHODS

We employ multiple-taper (MT) spectrum estimation (Thomson, 1982; Prieto and others, 2009), which suits coherence estimation well. Multitaper algorithms compute a finite set of statistically independent spectrum estimates $X^{(k)}(f)$, called eigenspectra, from a narrow spectral band about a target frequency f . The degrees-of-freedom (dof) in a coherence estimate $C(f)$ determine its confidence levels for nonrandomness (Abramowitz and Stegun, 1965; Thomson and others, 2007). The dof are determined by the time-bandwidth product p , which scales the estimation half-bandwidth $\Delta f = pf_R$ where $f_R = 1/T$ is the Rayleigh frequency of a time series with duration T . For a 50-year series, $f_R = 0.02$ cpy. For time-bandwidth product p , there are $2p - 1$ orthogonal Slepian data tapers $w^{(k)} = \{w_0^{(k)}, w_1^{(k)}, \dots, w_{N-1}^{(k)}\}$ that have useful spectral leakage properties. Given two data series $x = \{x_0, x_1, \dots, x_{N-1}\}$ and $y = \{y_0, y_1, \dots, y_{N-1}\}$ we compute spectrum estimates

$$\begin{aligned} X^{(k)}(f) &= \sum_{n=0}^{N-1} w_n^{(k)} x_n \exp(i2\pi fn\Delta t) \\ Y^{(k)}(f) &= \sum_{n=0}^{N-1} w_n^{(k)} y_n \exp(i2\pi fn\Delta t) \end{aligned} \quad (1)$$

for Slepian tapers indexed by $k = 0, 1, \dots, K - 1$, where $K \leq 2p - 1$. The coherence $C(f)$ is estimated via

$$C(f) = \frac{\sum_{k=0}^{K-1} (X^{(k)}(f))^* Y^{(k)}(f)}{\sqrt{\sum_{k=0}^{K-1} |X^{(k)}(f)|^2} \sqrt{\sum_{k=0}^{K-1} |Y^{(k)}(f)|^2}} \quad (2)$$

The mod-squared coherence $|C(f)|^2$ will have statistics related to the F variance-ratio test with 2 and $(2K - 2)$ degrees of freedom. The correlation transfer function (Park and Levin, 2000)

$$H(f) = \left(\sum_{k=0}^{K-1} (X^{(k)}(f))^* Y^{(k)}(f) \right) / \left(\sum_{k=0}^{K-1} |X^{(k)}(f)|^2 \right) \quad (3)$$

assumes that the process $\{x_n\}$ is a causal factor in the process $\{y_n\}$. Switching the variables X and Y reverses the assumed direction of causality. The online supplement to Park (2009) provides test data and computer code for some simple coherence and transfer function relationships: time lags, time leads, integral and derivative relationships, *et cetera*.

Both temperature and CO_2 time series have significant autoregressive memory and red spectra. We prewhiten all time series with a simple one-month first-difference (fig. 1). We difference the quasi-weekly GLOBALVIEW time series after shifting by four samples instead of one to preserve spectral relationships. For each time interval considered, we subtract the mean of the first-differenced series, which removes any original trend. We fit for periodic components at $f = 1$ and $f = 2$ cpy and subtract them. Because the yearly cycles of climate observations have some variability, the amplitudes of the fitted $f = 1$ and $f = 2$ cpy cosinusoids depend on the time interval studied. For 30-yr data series, we choose $p = 3.6$ and $K = 6$ Slepian tapers for spectrum estimation, so that the estimation half-bandwidth $\Delta f = 0.12$ cpy.

We computed a wavelet-based coherence estimator for selected data-series pairs, in order to investigate the transition in the coherence relationship reported by Park (2009). Similar to multiple-taper Fourier techniques, one can define a frequency-

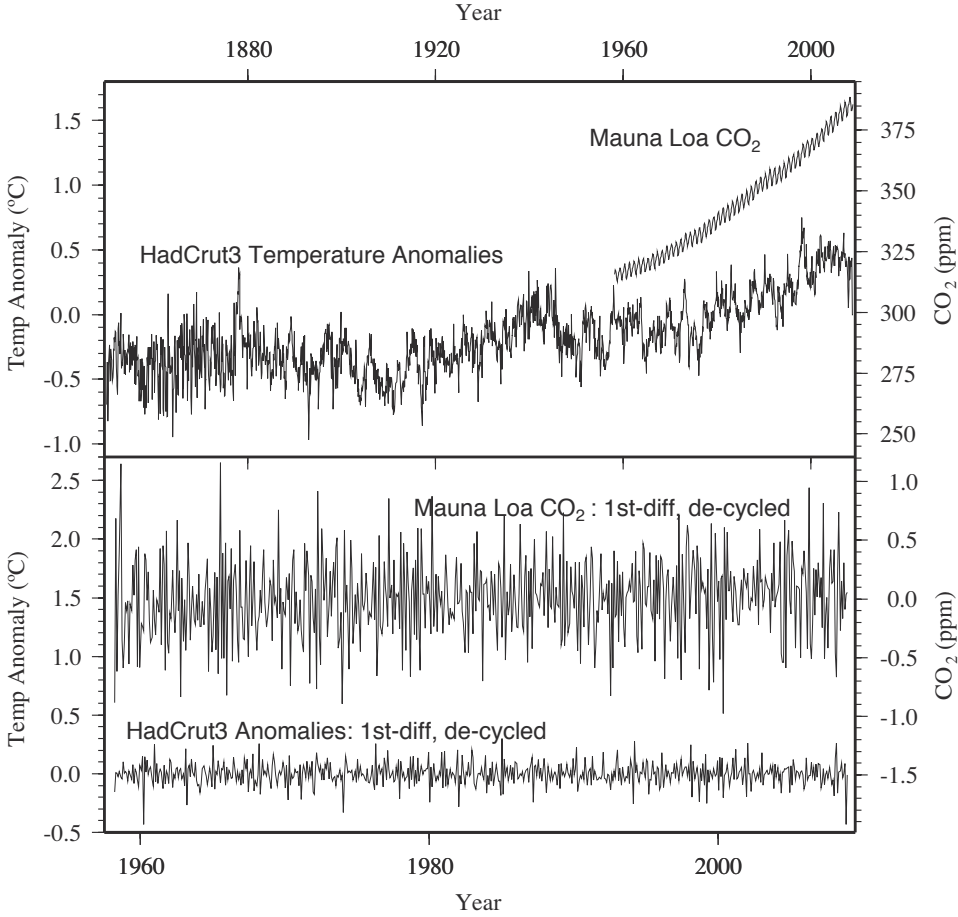


Fig. 1. Data used in this study. Upper: Global-average temperature-anomaly data from the Hadley Centre database (Brohan and others, 2006) since 1850 and CO₂ measured at Mauna Loa, Hawaii since 1958 (Keeling and others, 2009). Data are sampled monthly. Lower: Same datasets 1958–2008, after first-difference filter, demeaning, and subtraction of annual and semiannual cycles.

concentrated sequence of Slepian wavelets (Lilly and Park, 1995) that can be used for spectrum estimation. Multi-wavelet coherence has been applied to both seismology (Bear and Pavlis, 1999) and climate (Park and Mann, 2000; Koch and others, 2003) data analysis. The Slepian wavelets optimize spectral-leakage resistance in a user-defined bandwidth about a carrier frequency f_o , within a time interval that corresponds to a fixed number of cycles of period $T_o = 1/f_o$. The advantage of wavelets over so-called “evolutionary” spectrum estimates is that coherence can be estimated over a fixed number of cycles, rather than a fixed time interval. Aside from this distinction, the interpretation of wavelet-based coherence differs little from standard Fourier-transform approaches. In this study, we utilize Slepian wavelets of 4-cycle duration, time-bandwidth product $p = 2.5$, and use $K = 3$ wavelets to estimate time-varying spectra and coherence.

We also apply multivariate coherence estimators, in addition to coherence estimates between pairs of data series. Because the Slepian tapers are mutually orthogonal, the complex-valued eigenspectral estimates $Y^{(k)}(f)$ are statistically independent for

white noise time series, a property that can be exploited even where the underlying spectra are smoothly-varying, that is, locally white, in the frequency domain (Thomson, 1982). To discover band-limited correlated variability in a multivariate dataset of M data series, where $M > K$, we assemble an $M \times K$ matrix \mathbf{A} , where $A_{mk} = Y_m^{(k)}(f)$ is the k th eigenspectrum estimate at f of the m th data series. We compute the singular-value decomposition

$$\mathbf{A} = \sum_{k=1}^K \lambda_k \mathbf{u}_k \otimes \mathbf{v}_k^* \quad (4)$$

where the singular values $\lambda_1 \geq \lambda_2 \cdots \lambda_K \geq 0$ and the asterisk denotes complex conjugation (Mann and Park, 1999; Apipattanavis and others, 2009). The left-singular vector \mathbf{u}_k represents the relative amplitudes and phases of the M data series in the k th mode of correlated variability, that is, the k th empirical orthogonal function (EOF). The right-singular vector \mathbf{v}_k represents the narrowband spectral signature of the k th EOF.

Even the most sophisticated statistical methods can fail if their starting assumptions are incorrect. Statements such as “99 percent confidence for nonrandomness” are precisely valid only in their proper context. Multiple-taper spectrum estimates assume the time series to be stochastic and stationary (Thomson, 1982), and many tests for deterministic or nonstationary signals have been devised (Thomson, 1982, 1990; Thomson and others, 2007). Thomson (1997) reported that the global-average temperature time series fails tests for stationary behavior near $f = 0.25$ and $f = 0.5$ cyc/yr, probably due to long-term trends in, respectively, ENSO and the Quasi Biennial Oscillation (QBO, see Labitzke, 2005). Wavelet methods can be used to explore such nonstationarity, as we argue below. Unexpected biases to coherence estimates are possible if the data possess strong periodic or near-periodic signals, such as the 11-year and 22-year sunspot cycles, or if calendar effects alias 7-day work-week cycle into the monthly-averaged CO_2 data (Cleveland and Devlin, 1980). Because statistical assumptions can rarely be guaranteed 100 percent, conclusions from this study should motivate, rather than terminate, further investigation.

COHERENCE BETWEEN ATMOSPHERIC CO_2 AND GLOBAL TEMPERATURE

Park (2009) showed that $C(f)$ between Hadley-Centre global-average temperature and CO_2 -concentration at Mauna Loa USA over 1958 to 1988 agrees largely with Kuo and others, 1990, but coherence over 1979 to 2008 differs significantly (fig. 2). For 1958 to 1988 $|C(f)|^2$ exceeds the 99 percent confidence level for nonrandomness over $0.2 f < 0.6$ cpy, breaches the 90 percent confidence level for non-periodic variability near $f = 1$ cpy, and breaches the 90 percent confidence level within $1.25 f < 1.6$ cpy. For 1979 to 2008 $|C(f)|^2$ exceeds 99 percent confidence over a narrower low-frequency bandpass and displays near-zero coherence at $f = 1.0$ cpy.

The coherence phase $\arg(C(f))$ indicates a shift in the nature of the temperature- CO_2 linkage as well as in its strength. During 1958 to 1988 a linear phase ramp mimics the effect of a 6-month delay in CO_2 fluctuations relative to those in global ΔT . Kuo and others (1990) reported a 5-month delay; the discrepancy might relate to updates in the Hadley Centre SST dataset (Brohan and others, 2006). During 1979 to 2008 the interannual $\arg(C(f)) \sim 90^\circ$ where $|C(f)|^2$ is significant, that is, a constant phase rather than a phase ramp. The correlation transfer function $H(f)$ has amplitudes of 2 to 3 ppm/ $^\circ\text{C}$ over the bandwidth of high coherence at interannual frequencies, but the apparent transfer function for annualcycle fluctuation is substantially larger: 4 to 5 ppm/ $^\circ\text{C}$. The 90° phase relationship and the decreasing trend in $H(f)$ amplitude for $f < 1$ cpy are consistent with atmospheric CO_2 concentration behaving as a scaled integral of interannual global temperature fluctuations (Park, 2009).

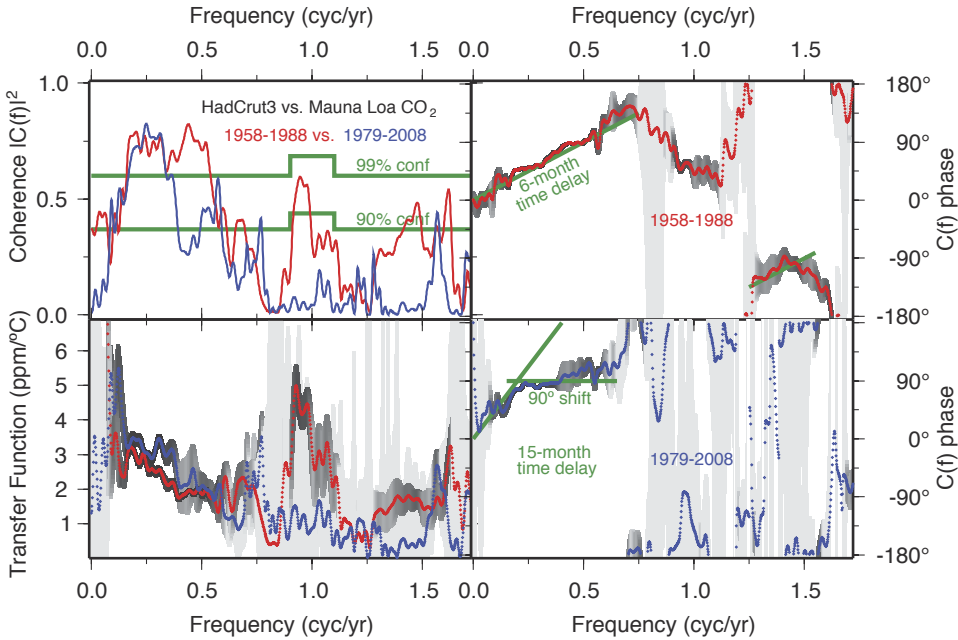


Fig. 2. Coherence between global-average temperature (Hadley-Centre time series) and monthly Mauna Loa CO₂ observations. Left panels compare squared coherence $|C(f)|^2$ and correlation transfer function $H(f)$ for 1958–1988 (red) and 1979–2008 (blue) time intervals. The 90% and 99% confidence intervals for 2 and 10 degrees of freedom (2 and 8 dof near the annual cycle) are plotted in green. Right panels plot the coherence phases for the two data intervals, with the phases of simple time-series relationships plotted in green. Uncertainty estimates for transfer function and coherence phase are plotted in grayshade, with lighter gray for larger uncertainties.

We supplement the Park (2009) coherence results to include global-average temperature estimates from sources beyond the Climate Research Unit at the University of East Anglia. The GISTEMP dataset of the NASA Goddard Institute for Space Studies offers a global-average data product computed from land-based surface-air temperature observations (Hansen and others, 1999), without information from SST measurements, either from ships or from satellites. The GISTEMP global-average data series coheres with the Mauna Loa CO₂ time series in a manner similar to HadCrut3 (fig. 3). Significant coherence at interannual frequencies is observed for both the 1958 to 1988 and 1979 to 2008 time intervals, with a marginally significant coherence (>90% confidence) in 1958 to 1988 for annual-cycle fluctuations. The correlation transfer function $|H(f)|$ falls in the ranges defined by the HadCrut3 data set, with a smoother decline in amplitude with increasing f in the interannual bandpass. The coherence phase $\arg(C(f))$ in figure 3 follows roughly the behavior seen in figure 2, but differences are significant, relative to the formal uncertainties on $\arg C(f)$. The expected 6-month phase ramp during 1958–1988 is choppy, and the interannual phase shift of CO₂ relative to GISTEMP during 1979 to 2008 is 60 to 75° rather than 90°. The latter discrepancy implies that interannual CO₂ fluctuations occur slightly ahead of a first-integral of GISTEMP temperature fluctuations. This can be explained if the principal source of CO₂-temperature coherence is related to SST fluctuations and their effect on atmosphere-ocean gas exchange, and that the land-based GISTEMP global average data series responds to SST variations with time lags of 2 to 4 months. Coherence estimates between the HadCrut3 and GISTEMP time series (not shown)

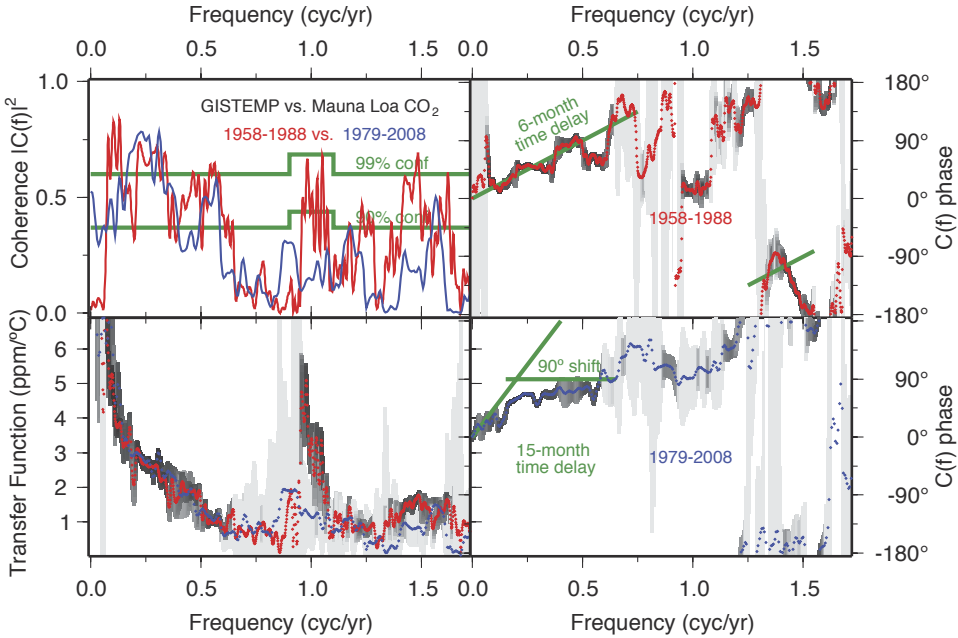


Fig. 3. Coherence between global-average temperature (NASA-GISS time series from meteorological stations) and monthly Mauna Loa CO_2 observations. Left panels compare squared coherence $|C(f)|^2$ and correlation transfer function $H(f)$ for 1958–1988 (red) and 1979–2008 (blue) time intervals. The 90% and 99% confidence intervals for 2 and 10 degrees of freedom (2 and 8 dof near the annual cycle) are plotted in green. Right panels plot the coherence phases for the two data intervals, with the phases of simple time-series relationships plotted in green. Uncertainty estimates for transfer function and coherence phase are plotted in grayshade, with lighter gray for larger uncertainties.

agree with this scenario. They reveal high, but not perfect coherence, that is, $|C(f)|^2$ above the 99 percent confidence level for nonrandomness, and an irregular coherence phase $\arg(C(f)) \sim 15$ to 30° .

Yet another estimation philosophy is represented by the MSS satellite data for lower-troposphere temperatures, in which pointwise surface temperature measurements are replaced by vertical integrals of inferred temperature in the lowest few kilometers of Earth's atmosphere (Spencer and Christy, 1990; Mears and others, 2003). Both sources of monthly global-average temperature data lead to coherence estimates with 1979 to 2008 Mauna Loa CO_2 that comport with results from the HadCrut3 data set, with deviations similar to those of the GISTEMP coherence estimates (fig. 4). Unlike the surface temperatures, lower-tropospheric temperatures are marginally coherent with Mauna Loa CO_2 at $0.6 f < 0.9$ cpy, far from the ENSO band, with correlation transfer function amplitude near $1 \text{ ppm}/^\circ\text{C}$. The tropospheric transfer function has 70 to 80° phase shift and lower amplitude in the ENSO band, compared to HadCrut3 surface measurements, consistent with a delay and a dampening of SST fluctuations with height above Earth's surface.

Differing CO_2 coherence among the different temperature data series could be due to many factors, including influences that involve other climate variables, for example, precipitation. Coherence with individual gridpoint time series in the HadCrut3 data set (see Appendix A) reveal strong coherence of CO_2 with interannual temperature variations in the open tropical ocean. pCO_2 surveys of the world ocean (Takahashi and others, 2002, 2009) show that low-latitude pCO_2 in the oceans exceeds

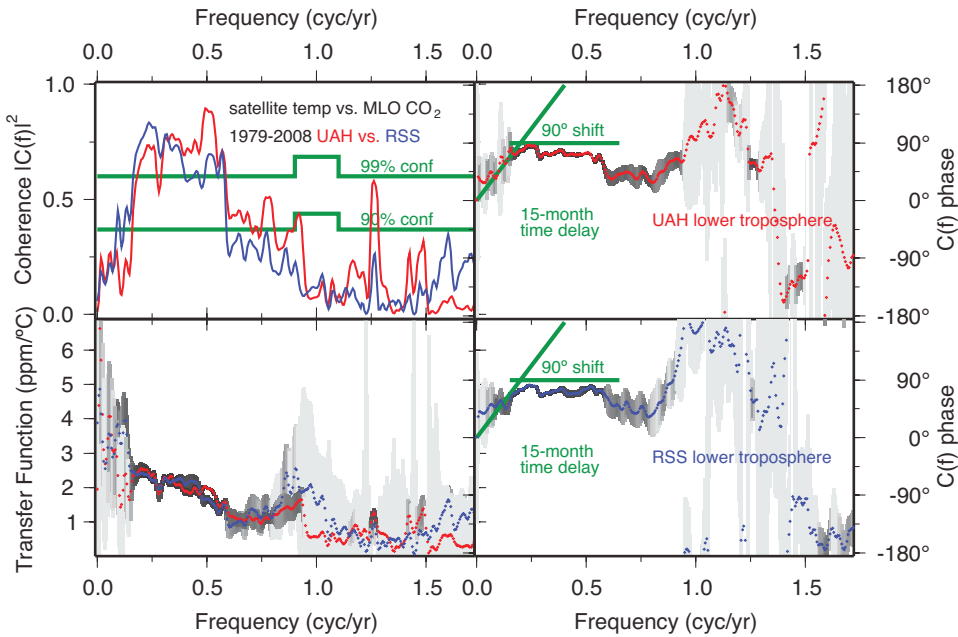


Fig. 4. Coherence between global-average lower troposphere temperature (Microwave Sounding Unit satellite) and monthly Mauna Loa CO₂ observations. Left panels compare squared coherence $|C(f)|^2$ and correlation transfer function $H(f)$ for 1979–2008 data interval obtained from Univ. Alabama-Huntsville (UAH, red) and Remote Sensing Systems (RSS, blue). The 90% and 99% confidence intervals for 2 and 10 degrees of freedom (2 and 8 dof near the annual cycle) are plotted in green. Right panels plot the coherence phases for the two data sources, with the phases of simple time-series relationships plotted in green. Uncertainty estimates for transfer function and coherence phase are plotted in grayshade, with lighter gray for larger uncertainties.

atmospheric CO₂ concentrations. The tropical oceans are therefore a source of CO₂ to the atmosphere; the net-positive ocean uptake of CO₂ is achieved via a larger carbon sink at high latitudes. Tropical SST increments should increment the pCO₂ imbalance and boost CO₂ flux from ocean to atmosphere in low latitudes, and figures 2 to 4 are consistent with this process. Physical controls on gas exchange are not the only factor to consider. Optical estimates of phytoplankton abundance suggest a negative correlation between tropical SST and biological utilization of dissolved CO₂ (Boyce and others, 2010). This poorly-calibrated but reinforcing biologic effect would boost surface-ocean pCO₂ and increase CO₂ flux to the atmosphere, reinforcing the effect of a temperature increase. Because the world ocean is currently a net carbon sink, a tropical SST increase effectively slows the net rate of oceanic CO₂-uptake.

WHEN AND HOW DID THE SHIFT IN COHERENCE PHASE OCCUR?

Restricting attention to Mauna Loa CO₂ and HadCrut3 global-average temperature, we apply multi-wavelet coherence analysis to investigate the evolution of interannual $\arg(C(f))$ (Lilly and Park, 1995; Park and Mann, 2000). Data series are first-differenced, demeaned and decycled at $f = 1$ and 2 cpy before computing the Slepian wavelet transform. Figure 5 demonstrates that coherence in the time-period domain is

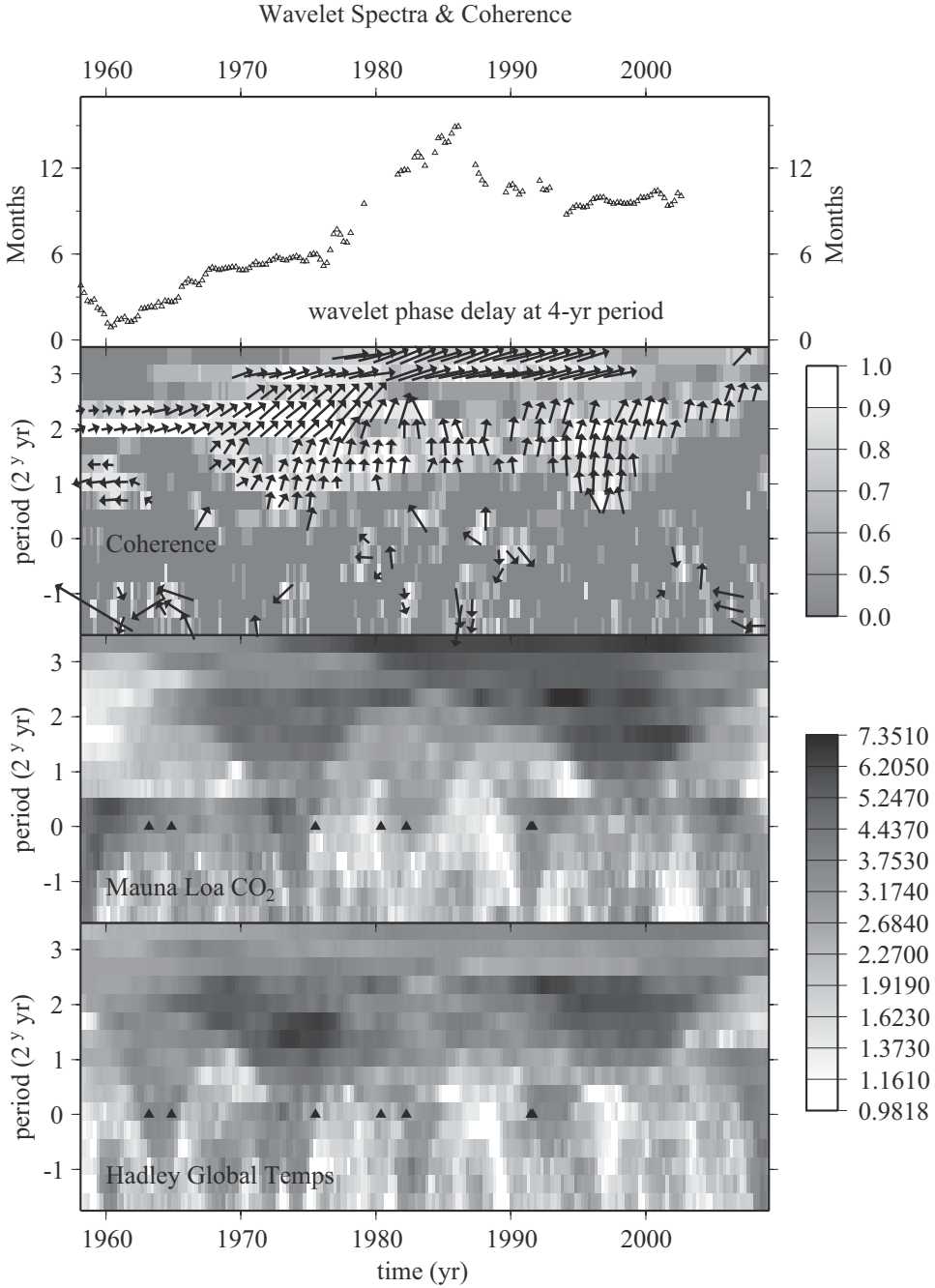


Fig. 5. Wavelet spectra and coherence for the Hadley-Centre global-average temperature and Mauna Loa CO₂ time series. Lower panels graph wavelet spectra in grayshade. The y-axes scale with the logarithm of wavelet period, in powers of two; darker shades imply larger spectrum values. Middle panel plots wavelet coherence, with lighter shades for larger $|C|^2$ values. For $|C(f)|^2 > 0.7$ we plot wavelet correlation as scaled arrows. A rightward arrow implies zero phase, and an up-arrow implies a 90° phase angle. Top panel graphs the time delay implied by the correlation phase for wavelets centered on 4-yr period, near the ENSO climate resonance.

most extensive during the ENSO episodes of the 1970s and the late 1990s, near maxima in the wavelet spectra for both CO₂ and temperature data series. Significant coherence is persistent for much of the 1958 to 2008 interval for wavelets at period $T = 4$ years, roughly the ENSO period. The phase of the wavelet coherence at 4-yr time scale, indicated by arrows at time-period points where $|C(f)|^2 > 0.70$, shows a noticeable shift near the year 1980. Translating this shift into a time-lag at 4-yr period (fig. 5A) the wavelet coherence phase-lag is observed to jump from ~ 6 months to ~ 12 to 15 months across a transition interval of 5 years. We observe depressed CO₂-temperature wavelet coherence during the transition. A peak 15-month phase lag for a 4-cycle (16-yr) time interval is found to be centered on the mid-1980s, after which the CO₂-temperature wavelet phase decreased to 10 to 12 months for time intervals centered in the 1990s and 2000s.

The $\arg(C(f))$ phase would increment monotonically if it were responding to a growing saturation of the oceanic carbon sink. Rather, a marked transition in the inter-annual CO₂-temperature phase is suggested in the late 1970s. This transition coincides with the oft-cited 1970s climate transition that heralded a 20-year secular rise in temperatures (Trenberth, 1990; Graham, 1994; Park and Mann, 2000; Meehl and others, 2009), following a 35-yr interval of stagnant temperatures in the Northern Hemisphere. Because the 1970s climate transition is commonly associated with a change in ocean circulation, as well as a polarity change in the Pacific Decadal Oscillation (PDO, see Mantua and Hare, 2002) it seems likely that the CO₂-temperature coherence transition identified by Park (2009) is associated with this event. Park and Mann (2000) found, via a multiwavelet analysis of an earlier version of the HadCrut gridded temperature data product (Jones and Briffa, 1992) that the spatio-temporal patterns of multicycle 20th-century ENSO episodes were multifarious, displaying global-average temperature fluctuations that varied greatly in amplitude from decade to decade. It is therefore not surprising that CO₂-temperature coherence phase shifted abruptly between the two largest ENSO episodes of the late 20th century.

COHERENCE BETWEEN ATMOSPHERIC CO₂, NAO AND SOI

Oceanic CO₂ uptake is large in the North Atlantic (Takahashi and others, 2009), but we do not find pervasive interannual coherence between atmospheric CO₂ time series and gridpoint temperatures in the region. Thickening of the surface mixed layer via wind stress is hypothesized to be more important than SST for CO₂-uptake in the North Atlantic, and the North Atlantic Oscillation, NAO, a normalized sea-level pressure index, correlates with storminess in the region (Hurrell and Deser, 2009). Because ENSO couples interannual temperature and circulation fluctuations, one expects to find coherence between the pressure-based Southern Oscillation Index (SOI) and atmospheric CO₂ with significance comparable to $C(f)$ with temperature time series. Unique features in SOI-CO₂ coherence amplitude and phase may offer clues to causal relations.

Figures 6A and 6B show the coherence between NAO and SOI is weak at most interannual frequencies during 1979 to 2008, demonstrating their status as independent climate proxies. To test overall coherence of NAO and SOI with CO₂ measurements, we averaged $|C(f)|^2$ for all 14 near-continuous GLOBALVIEW stations (fig. 6C). The average $|C(f)|^2 \sim 0.5$ for SOI for $0.2 f < 0.5$ cpy. Because the significance thresholds for multiple CO₂ records are lower than for single records (28 and 140 dof versus 2 and 10 dof), the average $|C(f)|^2$ for SOI exceeds the 99 percent confidence limit for nonrandomness for $0.15 f < 0.8$ cpy, a broader bandpass than typical for ENSO variability.

By contrast, average $|C(f)|^2$ for NAO fails to exceed 90 percent confidence for nonrandomness over most $f < 1.0$ cpy. The largest peak in average $|C(f)|^2$ for NAO occurs near $f = 0.35$ cpy, but near this frequency the NAO is strongly coherent with the

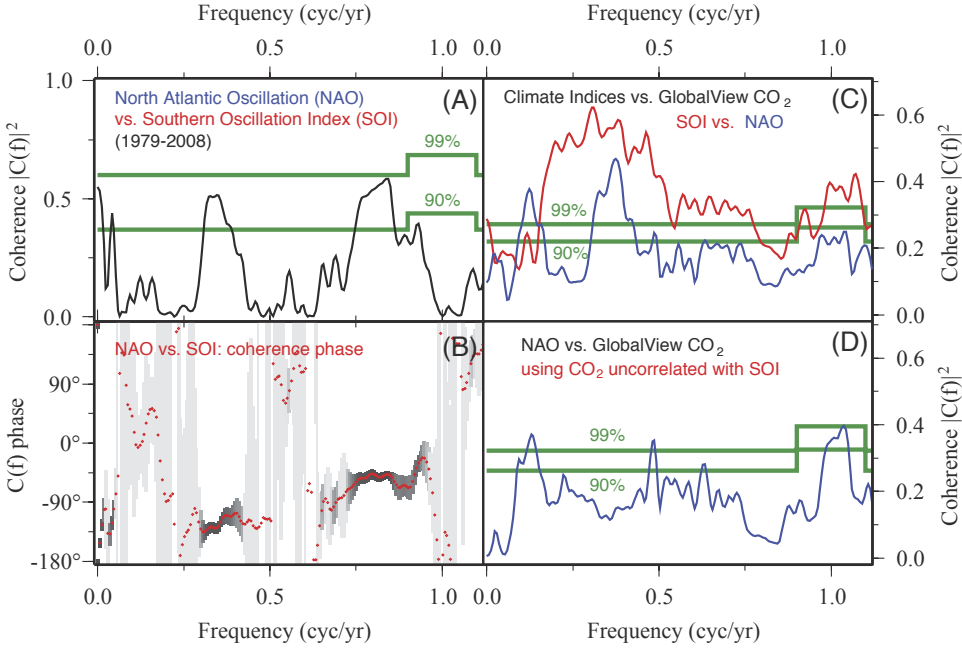


Fig. 6. Coherence between monthly values of the Southern Oscillation Index (SOI) and the North Atlantic Oscillation (NAO) and 14 long-running CO₂ GLOBALVIEW sites. (A) Interannual $|C(f)|^2$ between NAO and SOI for 1979–2008. The 90% and 99% confidence intervals for 2 and 10 degrees of freedom (2 and 8 dof near the annual cycle) are plotted in green. (B) The coherence phase $\arg(C(f))$ between NAO and SOI, with grayshaded uncertainties. (C) Summed squared coherences $|C(f)|^2$ between 14 GLOBALVIEW data series versus SOI (red) and NAO (blue). The 90% and 99% confidence intervals for 28 and 140 degrees of freedom (28 and 112 dof near the annual cycle) are plotted in green. (D) Summed squared coherences $|C(f)|^2$ between NAO and 14 GLOBALVIEW data series after subtraction of the CO₂ variance coherent with SOI. The 90% and 99% confidence intervals for 28 and 112 degrees of freedom (28 and 84 dof near the annual cycle) are plotted in green.

SOI. We subtracted the portion of the GLOBALVIEW CO₂ spectra that are coherent with the SOI and recomputed the coherence of the residuals with the NAO (fig. 6D). The coherence peak near $f = 0.35$ cpy disappears for this case, leaving only two $|C(f)|^2$ peaks that broach the 99 percent confidence level, near the annual frequency $f = 1$ cpy and at $f = 0.13$ cpy. Mann and Park (1994, 1996) found a mode of correlated variability near $f = 0.13$ cpy in global-gridded temperatures and in joint temperature-pressure data sets at 95 percent confidence for nonrandomness. Mann and Park (1994) reported that the spatial pattern of this 7 to 8-yr period mode of variability resembled the quasi-biennial oscillation, QBO, centered around the North Atlantic. This corroboration suggests that the $f = 0.13$ cpy peak in average $|C(f)|^2$ between NAO and the GLOBALVIEW CO₂ data for 1979 to 2008 represents a meaningful natural climate process.

The correlation amplitudes and phases at selected frequencies [see eq (3)] lend support to meaningful correlation between SOI, NAO and CO₂ fluctuations (fig. 7). Phased coherence $C(f)$ for SOI at the ENSO frequency $f = 0.25$ cpy shows a consistent pattern, except for outlier station **cmn** (fig. 7B). At $f = 0.13$ cpy, NAO fails to cohere with two stations, **brw** (Barrow, Alaska) and **nwr** (Niwot Ridge, Colorado), but exhibits consistent phase angles at the remaining stations (fig. 7C). Near-identical correlation coefficients at interannual frequencies (figs. 7B and 7C) seem consistent with a widespread interannual causal factor, that is, the ocean. Long-term CO₂ fluctuations

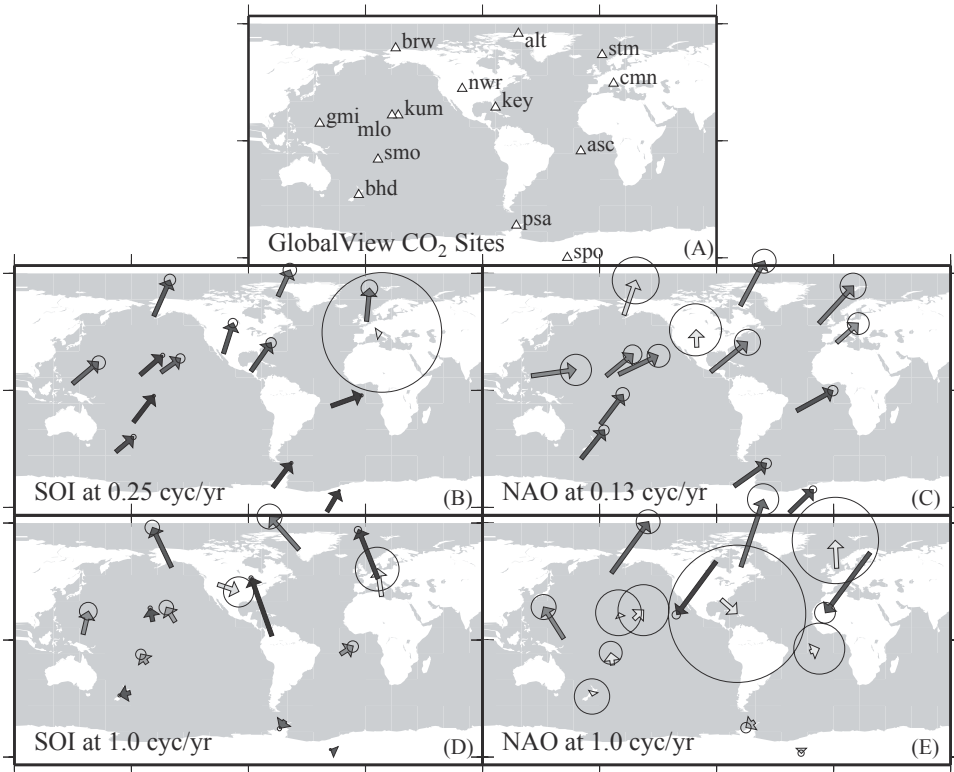


Fig. 7. Geographic correlation pattern between NAO, SOI and 14 GLOBALVIEW CO_2 sites for 1979–2008 at selected frequencies: (A) locations of 14 GLOBALVIEW stations; (B) transfer function for SOI at $f = 0.25$ cpy. Length of arrow scales correlation value. Darker arrow shades indicate higher coherence. Circles indicate uncertainty of transfer function. Eastward arrow is 0° phase. Upward arrow is 90° phase. (C) Transfer function for NAO at $f = 0.13$ cpy. (D) Transfer function for SOI at $f = 1.00$ cpy. (E) Transfer function for NAO at $f = 1.00$ cpy.

are hypothetically linked to North Atlantic Deep Water formation as part of the conveyor-belt hypothesis for Pleistocene glacial cycles (Maasch and Saltzman, 1990). Our result suggests that fluctuations in this process may be observable on decadal time scales.

At $f = 1$ cpy, both SOI and NAO appear to cohere significantly with the residual CO_2 variability after a fixed annual cycle is subtracted, with the largest correlation coefficients at GLOBALVIEW stations in North America and Europe (figs. 7D and 7E). Correlation phases for SOI for annual-cycle variability are near-parallel. Correlation phases for NAO alternate polarity across continents and/or oceans. The diverse sizes of correlation coefficients for the $f = 1$ cpy residuals argue for a more localized annual-cycle causal factor, for example, the Northern-Hemisphere forests.

The coherence of SOI with both global temperatures and with the Mauna Loa CO_2 record exhibits differing phase lags between the mid- and late-20th century, consistent with a major climate shift in the late 1970s. The SOI tends to be negatively correlated with tropical SST fluctuations (McPhaden and others, 2006) and during 1979 to 2008 it also exhibited a phase advance of roughly 6 months for $0.2 < f < 0.5$ cpy (fig. 8). The phase ramp deviates for $f > 0.5$ cpy, outside the ENSO bandpass. Phase complexities are absent for coherence between HadCrut3 temperatures and SOI for the 1951 to 1980 interval (fig. 9), for which the interannual $\arg(C(f)) \sim 150^\circ$. We

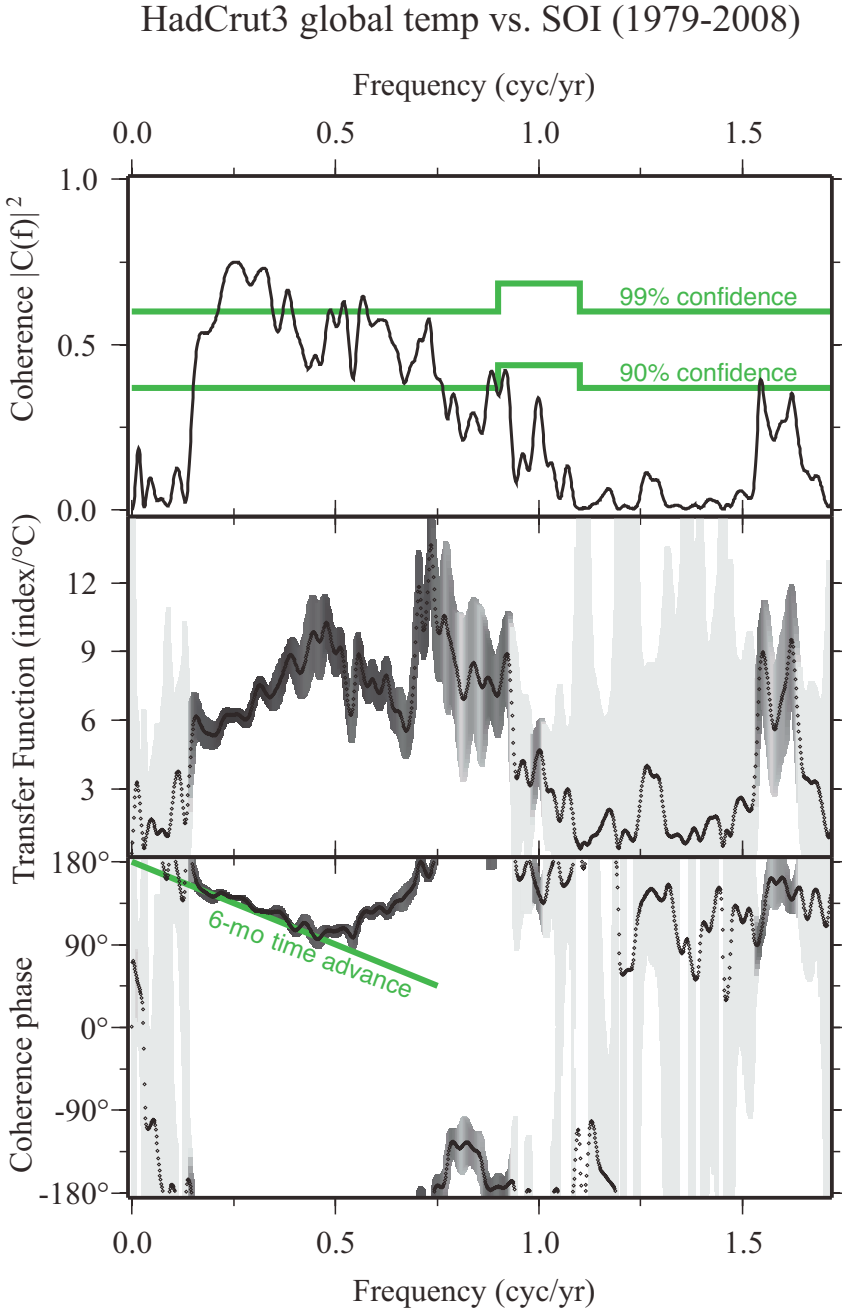


Fig. 8. Coherence between monthly global-average temperature (Hadley-Centre values) and the Southern Oscillation Index (SOI) for 1979–2008. Upper: interannual $|C(f)|^2$, with the 90% and 99% confidence intervals for 2 and 10 degrees of freedom (2 and 8 dof near the annual cycle) plotted in green. Center: Transfer-function amplitude with grayshade uncertainties. Lower: Coherence phase with grayshade uncertainties. SOI is negatively correlated with global-average temperature, but deviates from a 180° phase lag along a phase ramp (green line) that indicates a 6-month time lead for SOI.

HadCrut3 global temp vs. SOI (1951-1980)

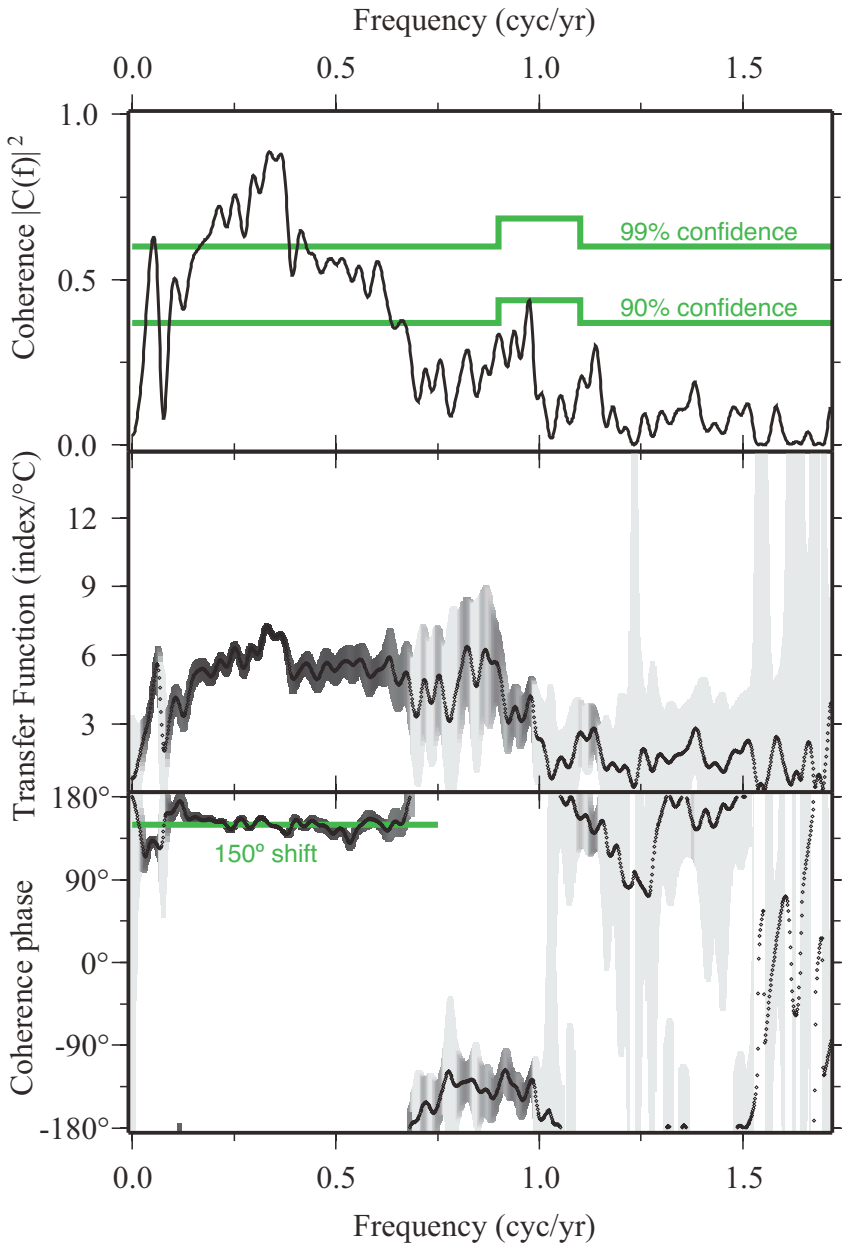


Fig. 9. Coherence between monthly global-average temperature (Hadley-Centre values) and the Southern Oscillation Index (SOI) for 1951–1980, mainly prior to the late 1970s climate transition. Upper: interannual $|C(f)|^2$, with the 90% and 99% confidence intervals for 2 and 10 degrees of freedom (2 and 8 dof near the annual cycle) plotted in green. Center: Transfer-function amplitude with grayshade uncertainties. Lower: Coherence phase with grayshade uncertainties. SOI is approximately negatively correlated with global-average temperature, but follows a 150° phase lag (green line) rather than 180°.

conclude that the late-1970s climate transition altered the correlation phase of SOI and ENSO-related SST fluctuations.

The coherence of SOI with Mauna Loa CO₂ also undergoes a shift between the 1958 to 1988 and 1979 to 2008 time intervals (figs. 10 and 11). In the ENSO bandpass (0.2-0.5 cpy) the shift does not have a simple time-domain analog. However, outside the ENSO bandpass the SOI coherence with Mauna Loa CO₂ has simpler phase, in particular, $\arg(C(f)) \sim 0^\circ$ for $0.5 f < 0.75$ cpy, even where 90 to 99 percent confidence for nonrandomness is not satisfied. We conclude that Mauna Loa CO₂ correlates more simply with temperature in the interannual ENSO bandpass, and more simply with pressure-based climate variables both above (via SOI) and below (via NAO) the ENSO bandpass.

Coherence with the annual-cycle residual switches from $\arg(C(f)) \sim -90^\circ$ in 1958 to 1988 to $\arg(C(f)) \sim 0^\circ$ in 1979 to 2008. This last transition suggests a positive correlation between SOI and CO₂ annual-cycle fluctuations before the late 1970s climate transition, and a negative correlation between SOI and the time-derivative of the CO₂ annual-cycle residual after the transition. Even though the quasi-annual correlation amplitude is relatively large and the phase relation simple, a causal factor is not obvious to us.

DISCUSSION

Occam's Razor is not a perfect tool, but a focus on the simplest observational relationships is often useful for generating and testing hypotheses. We have used the tools of spectrum analysis to explore relationships between Earth's carbon cycle and its climate system on time scales of one year and longer. The coherence $C(f)$ tests whether two time series are correlated near frequency f to varying degrees of statistical confidence. The coherence phase $\arg(C(f))$ can test causal relationships between time series. Simple phase ramps and phase shifts in the frequency domain correspond to simple models in the time domain that are not always detected with time-domain correlation techniques. Computer codes that demonstrate these relationships can be downloaded from the online supplement to Park (2009). For instance, a phase ramp in the frequency domain corresponds to a lead or lag in the time domain, and this behavior can be detected with a lagged correlation in the time domain. However, a 90° phase relationship will likely be undetected in the time domain, because a broadband signal and its derivative often do not have the same shape. In addition, a coherence relationship that changes with frequency is more difficult to detect with a time-domain correlation, which typically is dominated by the time scale with largest amplitude.

Our analysis demonstrates subtle, but significant, changes in the relationship between Earth's climate and atmospheric CO₂ in the late 20th century, extending the results of Park (2009). The earlier study found a shift in the coherence between the monthly global-average Hadley Centre temperature-anomaly data set (Brohan and others, 2006) and monthly Mauna Loa CO₂ observations (Keeling, 2008). Park (2009) hypothesized that a transition from a 6-month time lag (for 1958-1988) to a 15-month time lag (for 1979-2008) reflected a more-sluggish response of atmosphere-ocean CO₂-exchange to SST fluctuations in the late 20th century, supporting model-based estimates of a weakening oceanic carbon sink (Le Quere and others, 2007; Schuster and others, 2009; Khatiwala and others, 2009); see Knorr (2009) for a dissenting view. In this study we corroborate the transition, but use wavelet coherence to reject a gradual transition via oceanic saturation. We infer instead a rapid transition coinciding with the late-1970s climate shift near the most-recent inflection point for secular change in the global-average temperature (Trenberth, 1990; Graham, 1994; Park and Mann, 2000; Meehl and others, 2009). Parallel coherence estimates using the pressure-based Southern Oscillation Index (SOI) corroborate the notion of a carbon-cycle shift coeval with the climate shift, and add detail to the picture.

SOI vs. Mauna Loa CO₂ (1979-2008)

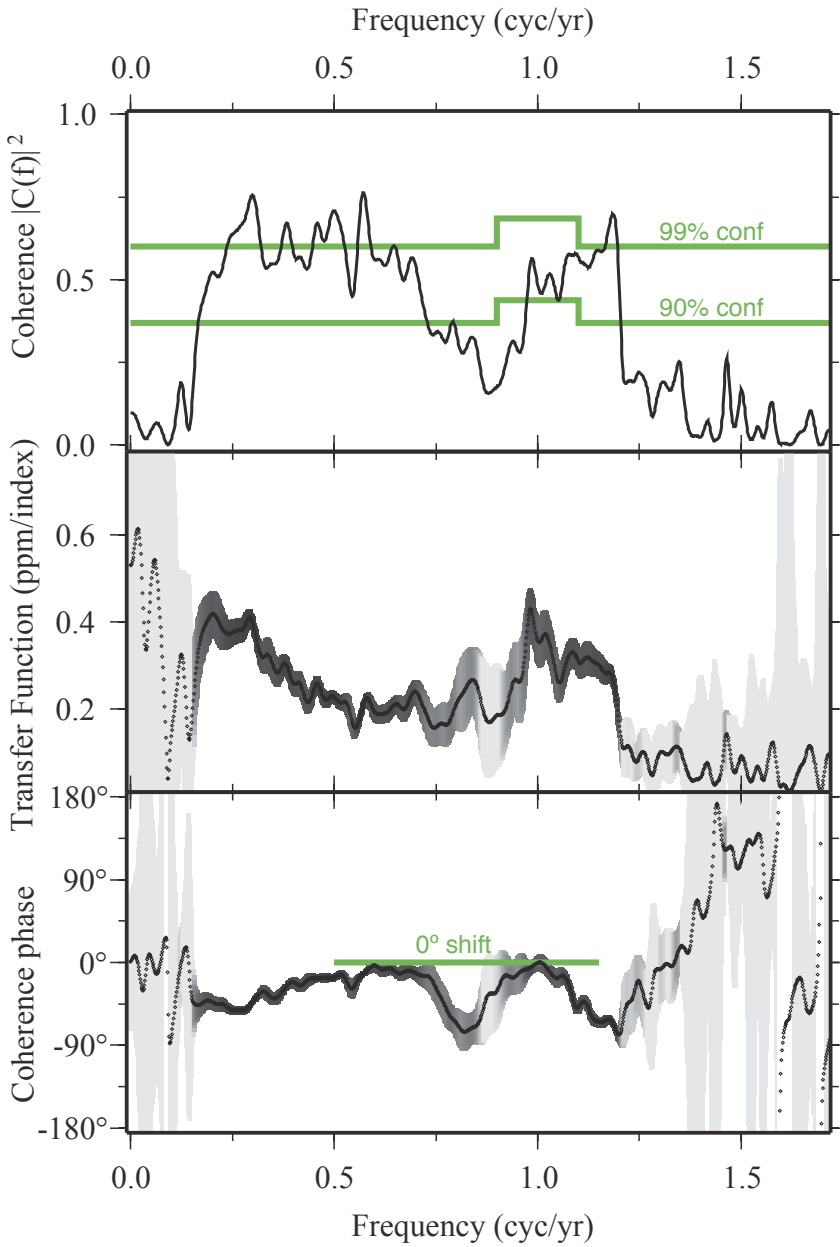


Fig. 10. Coherence between the Southern Oscillation Index (SOI) and monthly Mauna Loa CO₂ observations for 1979–2008. Upper: interannual $|C(f)|^2$, with the 90% and 99% confidence intervals for 2 and 10 degrees of freedom (2 and 8 dof near the annual cycle) plotted in green. Center: Transfer-function amplitude with grayshade uncertainties. Lower: Coherence phase with grayshade uncertainties. SOI is positively correlated with Mauna Loa CO₂ at both interannual and annual frequencies, but deviates from a 0° phase lag in the ENSO bandpass.

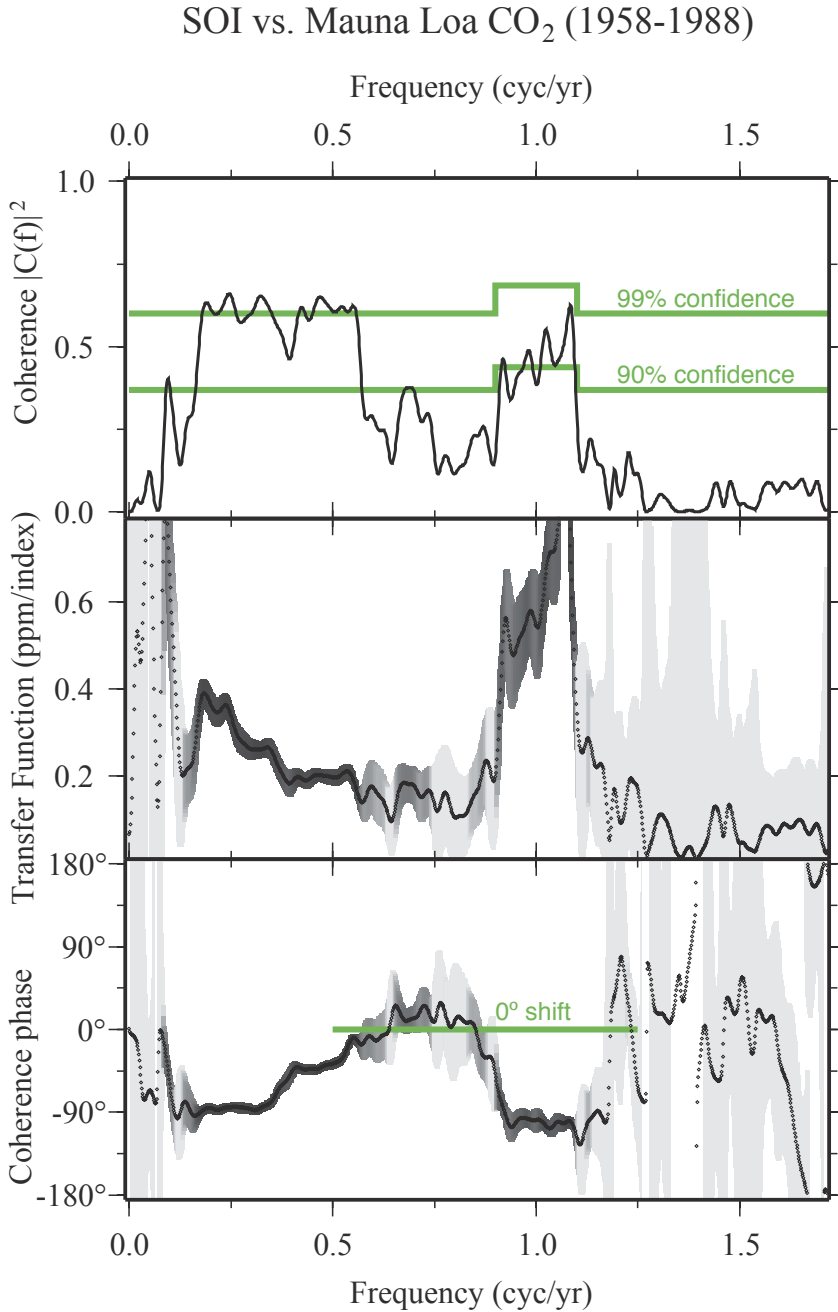


Fig. 11. Coherence between the Southern Oscillation Index (SOI) and monthly Mauna Loa CO₂ observations for 1958–1988. Upper: interannual $|C(f)|^2$, with the 90% and 99% confidence intervals for 2 and 10 degrees of freedom (2 and 8 dof near the annual cycle) plotted in green. Center: Transfer-function amplitude with grayshade uncertainties. Lower: Coherence phase with grayshade uncertainties. SOI is positively correlated with Mauna Loa CO₂ at interannual frequencies, but deviates from a 0° phase lag in the ENSO bandpass. At 90% confidence for nonrandomness, SOI exhibits a -90° phase shift for coherence of annual-cycle fluctuations, with large-amplitude transfer function.

In contrast to many studies in which interannual CO₂ fluctuations are explained primarily by means of a fluctuating appetite for carbon in the terrestrial biosphere (Lee and others, 1998; Bousquet and others, 2000; Zeng and others, 2005; Buermann and others, 2007; Qian and others, 2008), we argue that oceanic climate and carbon-cycle exchanges are a principal driver. By “a principal driver” we do not mean the ocean is the only agent, because terrestrial CO₂ flux is clearly evident in the spatial variation of data coherences described in Appendix A, and modeling studies predict substantial fluctuations in the terrestrial carbon cycle. However, temperature data restricted to continental interiors correlate more weakly with interannual CO₂ variability, as illustrated in Appendix A.

Evidence for simple coherence between interannual CO₂ variations and ocean climate indices includes (1) a simple ramp in the coherence phase $\arg(C(f))$ with Hadley-Centre global-average temperatures during 1958 to 1988 at frequencies $f \approx 0.5$ cpy, consistent with a 6-month lagged response; (2) a 90°-phase in the 1979 to 2008 interval, consistent with a direct correlation between oceanic SST and CO₂ rate-of-change; (3) the transition between these two relationships occurs near a recognized shift in Pacific ocean circulation in the late 1970s; (4) significant coherence between interannual CO₂ fluctuations at many GLOBALVIEW stations and low-latitude oceanic gridpoint temperatures in the Hadley-Centre dataset, with consistent correlation phases among different CO₂ stations; (5) coherences at >90 percent confidence for nonrandomness between the pressure-related SOI and NAO indices in frequency bands above and below, respectively, the ENSO bandpass; (6) zero-phase coherence for SOI above the ENSO band, and a geographic consistency in NAO coherence phase at 7-yr period, which is a recognized decadal mode of temperature variability; (7) when correlations are sought between CO₂ and global-temperature time series that do not involve sea-surface temperatures explicitly, based either on weather station (NASA-GISS) or satellite lower-troposphere (MSU) measurements, the coherence phase is perturbed, consistent with a downstream response to SST.

We suggest that oceanic control of CO₂ fluctuations relates to SST and wind-stress modulation of the mixed-layer thickness in different frequency passbands. In the ENSO band the simpler coherence-phase with CO₂ occurs for global-average temperature, not the pressure indices, pointing toward SST as the primary agent of CO₂ flux tied to ENSO, rather than pressure-induced atmospheric circulation changes.

We find scattered and inconsistent evidence for the coherence of interannual CO₂ fluctuations with continental temperature, in the Hadley-Center gridpoint time series. The terrestrial carbon cycle may be influenced more by drought than by temperature, however. Interannual drought fluctuations are closely tied to ENSO, and therefore closely tied to SST (Apipattanavis and others, 2009). The principal component of CO₂ variability at $f = 0.25$ cpy, in the 1979 to 2008 GLOBALVIEW marine-boundary-layer data product (see Appendix A) has peak amplitude in the mid- to high-latitude Northern Hemisphere with a 4-month time lag relative to the tropics and the Southern Hemisphere. Park (2009) noted a similar phase relationship that contrasted interannual CO₂ fluctuations at low latitude Mauna Loa, Hawaii from those at high-latitude Barrow, Alaska. The amplitude and phase lag argue for a prominent contribution by the extratropical terrestrial biosphere, but as a lagged response to oceanic SST variations. Our analysis does not exclude the possibility that the tropical terrestrial biosphere plays a major role in interannual CO₂ fluctuations via drought and fire (Page and others, 2002; McPhaden and others, 2006) but terrestrial influence would need to combine with oceanic low-latitude carbon-cycle processes to produce simple coherence relationships with oceanic climate indices.

Knowing where carbon moves in the natural system is a pre-requisite to forecasting mankind's inevitable meddling in the cycle. Statistical studies like this cannot uniquely determine the causes of the correlations that are detected. Rather, they serve as experimental data for the falsification of scientific hypotheses, in particular the predictions of global carbon-cycle models. Because the natural variability of climate and of climate models is substantial, long-term statistical relationships are better tools for validating theoretical relationships than are curve-fitting experiments that involve a few years of data. Now that CO₂ time series extend past a few decades, such statistical relationships can be better constrained.

ACKNOWLEDGMENTS

Reviewer comments by David J. Thomson of Queens University and one anonymous referee were helpful. This work was supported by the Yale Institute for Biospheric Studies.

APPENDIX A

SPATIAL PATTERNS OF CO₂-TEMPERATURE COHERENCE IN THE ENSO BAND

Park (2009) showed that interannual coherence between CO₂ and global-average temperature can be found at widely separated locations, Mauna Loa, Hawaii; Barrow, Alaska; South Pole, but with differences in transfer-function amplitude and phase. For coherence since 1979, the GLOBALVIEW data product (Masarie and Tans, 1995; GLOBALVIEW-CO₂, 2009) offers a wider selection of station locations to explore these statistical relationships. We restrict attention to 14 recording locations where CO₂ data series have data gaps, interpolated via the GLOBALVIEW averaging procedure, that total no more than two years out of the 30 years possible (table 1). Of these data series, only one fails to exhibit significant coherence with the HadCrut3 global-average temperature series at interannual frequencies $f < 0.5$ cpy: station **cmn**, a high-altitude site at Mt. Cimone, Italy.

We show station triplets in common latitude ranges. Figure 12 shows low- to mid-latitude Northern-Hemisphere stations. Figure 13 shows high-latitude Northern-Hemisphere stations. Figure 14 shows Southern-Hemisphere stations. With some variability, the GLOBALVIEW stations in figures 12 and 14 show significant coherence with global temperature, often exceeding 99 percent confidence for non-randomness, for $0.15 f < 0.5$ cpy, with coherence phase close to 90°. High-latitude NH stations show similar $|C(f)|^2$ behavior, with a modest, but significant, phase shift. At frequencies $f > 0.5$ cpy significant coherence is either absent or

TABLE 1

Long-running CO₂ observation sites in the GLOBALVIEW-CO₂ data product

| Station | Lat | Long | Elev (m) | Location |
|---------|--------|---------|----------|----------------------------|
| alt | 82.45 | -62.51 | 210 | Alert, Nunavut, Canada |
| asc | -7.92 | -14.42 | 54 | Ascension Is., UK |
| cmn | 44.18 | 10.70 | 2165 | Mt. Cimone, Italy |
| brw | 71.32 | -156.61 | 11 | Barrow, AK, USA |
| gmi | 13.43 | 144.78 | 6 | Guam, USA |
| key | 25.67 | -80.16 | 3 | Key Biscayne, FL, USA |
| kum | 19.52 | -154.82 | 3 | Cape Kumukahi, HI, USA |
| mlo | 19.54 | -155.58 | 3397 | Mauna Loa, HI, USA |
| nwr | 40.05 | -105.58 | 3526 | Niwot Ridge, CO, USA |
| psa | -64.92 | -64.00 | 10 | Palmer Station, Antarctica |
| smo | -14.25 | -170.56 | 42 | Tutuila, American Samoa |
| bhd - | -41.41 | 174.87 | 80 | Baring Head Station, NZ |
| spo | -89.98 | -24.80 | 2810 | South Pole, Antarctica |
| stm | 66.00 | 2.00 | 5 | Ocean Station M, Norway |

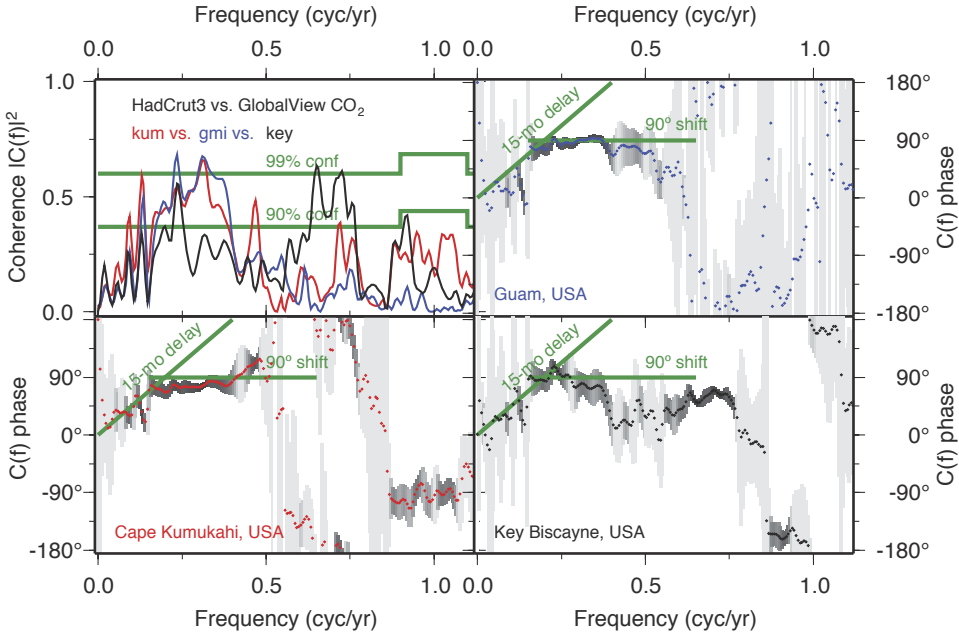


Fig. 12. Coherence between monthly global-average temperature (Hadley-Centre time series) and quasi-weekly CO_2 observations at low- and mid-latitude GLOBALVIEW stations **kum** (Cape Kumakahi, Hawaii; red), **gmi**, (Guam, USA; blue) and **key** (Key Biscayne, Florida; black). The 90% and 99% confidence intervals for 2 and 10 degrees of freedom (2 and 8 dof near the annual cycle) are plotted in green. Upper-left panel compares squared coherence $|C(f)|^2$ for the 1979–2008 time interval. Surrounding panels plot the coherence phases for the three stations, with the phases of simple time-series relationships plotted in green. Uncertainty estimates for coherence phase are plotted in grayshade, with lighter gray for larger uncertainties.

exhibits diverse values of coherence phase (stations **key**, **alt**, **brw**, **sno**, and **bhd**). This frequency dependence reinforces the notion that interannual variations in CO_2 are causally related to ENSO variability.

Park (2009) estimated coherence between Mauna Loa CO_2 and gridpoint temperature anomaly data over the time period 1958 to 2008, with largest $|C(f)|^2$ in the tropical oceans. Figure 15 shows similar behavior for widely-separated stations **alt** (Alert, Canada), **key** (Key Biscayne, USA) and **psa** (Palmer Station, Antarctica) for the period 1979 to 2008 at the ENSO frequency $f = 0.25$ cpy. The highest coherences in the tropical ocean are for **psa**, with values breaching 99 percent confidence for nonrandomness clustered broadly in the western Pacific and Indian oceans, which comprise opposing loci of large ENSO SST fluctuations. Although CO_2 data from both stations **key** and **alt** exhibit significant coherence with tropical-ocean gridpoints as well, it is smaller, with an altered geographical pattern. In addition, significant $|C(f)|^2$ for **key** and **alt** is found for clusters of gridpoints in the Northern Hemisphere, such as high-latitude North America (for **key**) and the North Pacific (for **alt**). Carbon exchange in the North Pacific switches sign both laterally and during the annual cycle (Takahashi and others, 2009, see figs. 9 and 15), and therefore may be more sensitive to interannual SST fluctuations than the high-latitude North Atlantic, where persistent CO_2 -uptake is influenced more by storminess fluctuations.

Figure 16 shows the phased transfer function between CO_2 and the HadCrut3 gridded temperature time series at the ENSO frequency $f = 0.25$ cpy. The arrows point east for positive correlation, west for negative correlation, and north for a 90° phase shift in the transfer function. Note that, despite station-by-station variations in coherence $|C(f)|^2$ among gridpoints in the HadCrut3 data set, the geographical patterns in the transfer function $H(f)$ are similar among stations **alt**, **key** and **psa**. For example, phase shifts near 90° characterize transfer functions $H(f)$ in the equatorial Indian Ocean, the Caribbean Sea and in the equatorial Atlantic off Brazil. Although $|C(f)|^2$ is significant in the climatically-sensitive eastern tropical Pacific, the transfer function $H(f)$ is small for gridpoints along the equator itself.

High $|C(f)|^2$ between ocean SST and atmospheric CO_2 suggests that ocean-atmosphere CO_2 flux is the determining factor in interannual CO_2 variations, but correlated factors are also relevant, such as precipita-

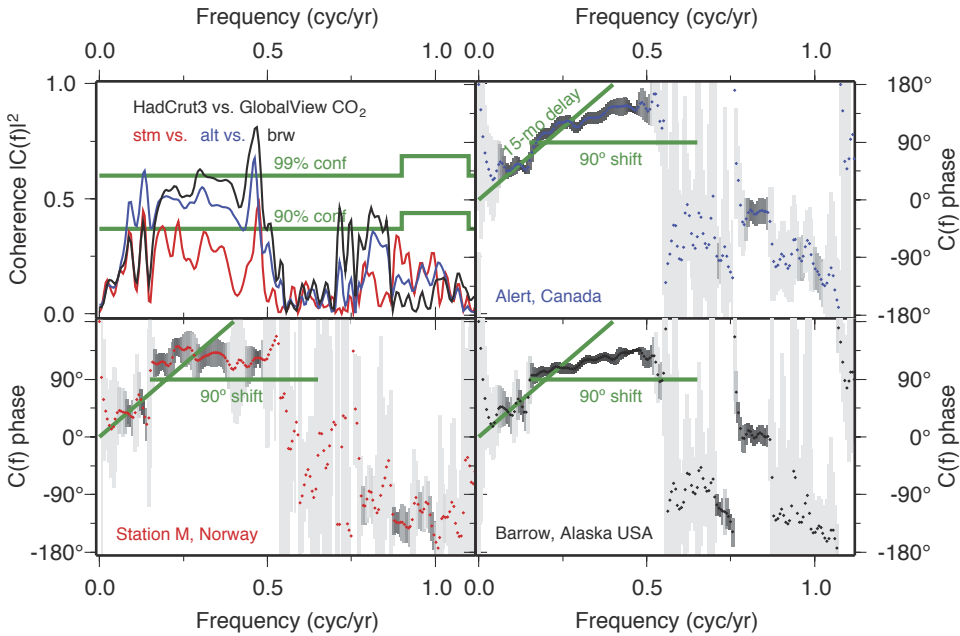


Fig. 13. Coherence between monthly global-average temperature (Hadley-Centre time series) and quasi-weekly CO₂ observations at high-latitude GLOBALVIEW stations **stm** (Station M, Norway; red), **alt** (Alert, Canada; blue) and **brw** (Barrow, Alaska; black), for the 1979–2008 time interval. Plotting conventions identical to figure 12.

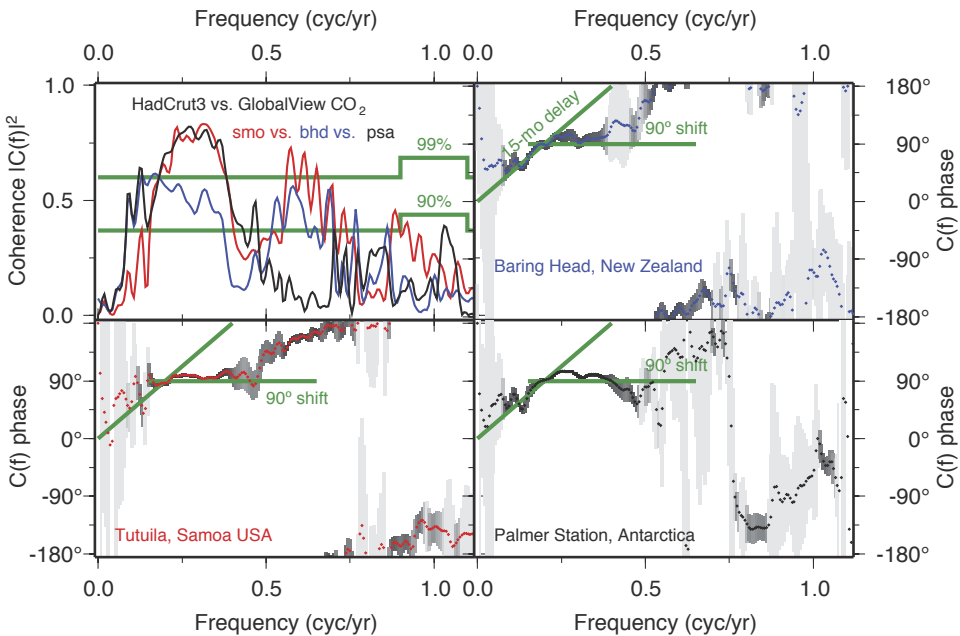


Fig. 14. Coherence between monthly global-average temperature (Hadley-Centre time series) and quasi-weekly CO₂ observations at Southern-Hemisphere GLOBALVIEW stations **smo** (Samoa, USA; red), **bhd** (Baring Head, New Zealand; blue) and **psa** (Palmer Station, Antarctica; black), for the 1979–2008 time interval. Plotting conventions identical to figure 12.

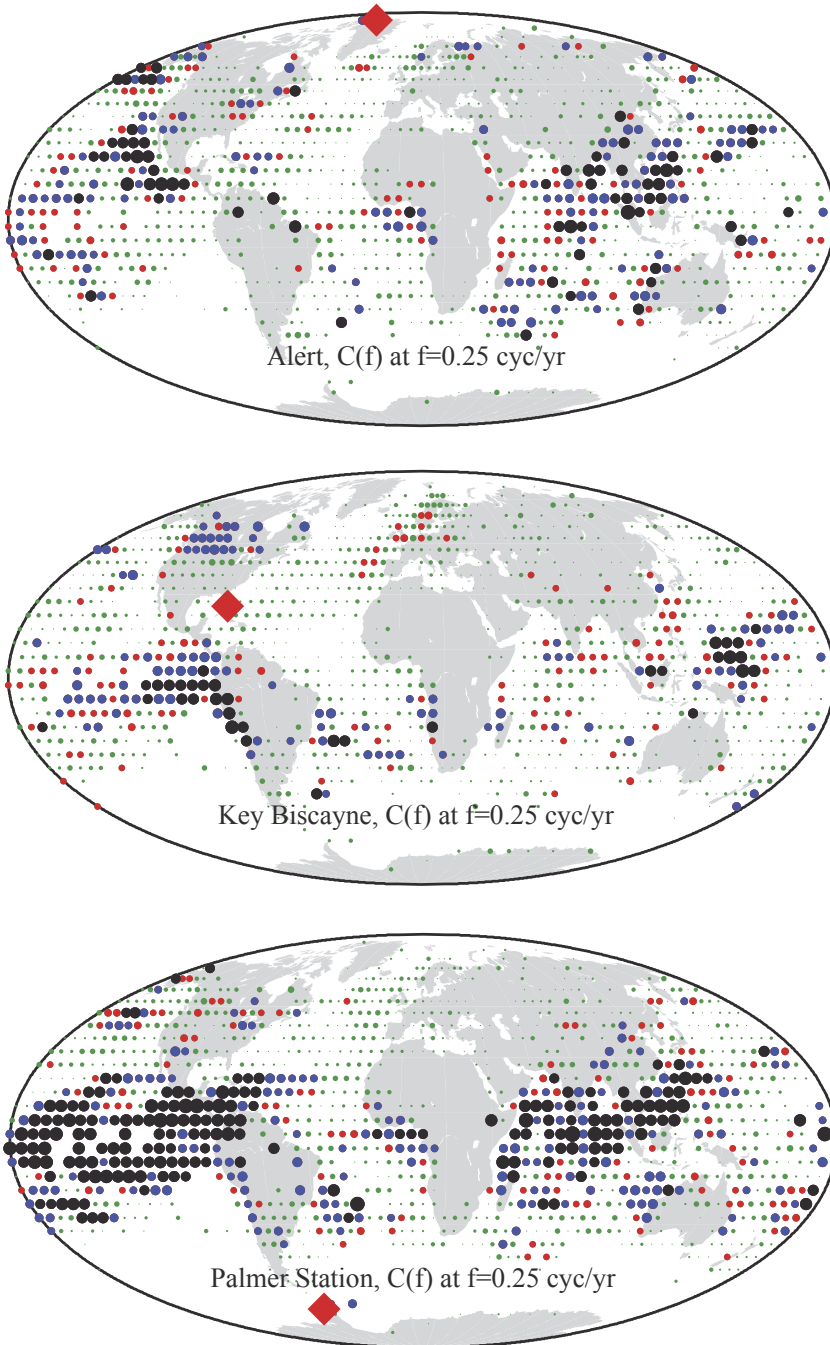


Fig. 15. Coherence between monthly gridpoint temperature anomalies (Hadley-Centre time series) and quasi-weekly CO₂ observations at GLOBALVIEW stations **alt** (Alert, Canada), **key** (Key Biscayne, Florida) and **psa** (Palmer Station, Antarctica), at ENSO bandpass $f = 0.25$ cpy for the 1979–2008 time interval. Symbol size proportional to coherence $|C(f)|^2$, with black circles $>99\%$ confidence for nonrandomness, blue circles $>95\%$ confidence, red circles $>90\%$ confidence, green circles $<90\%$ confidence.

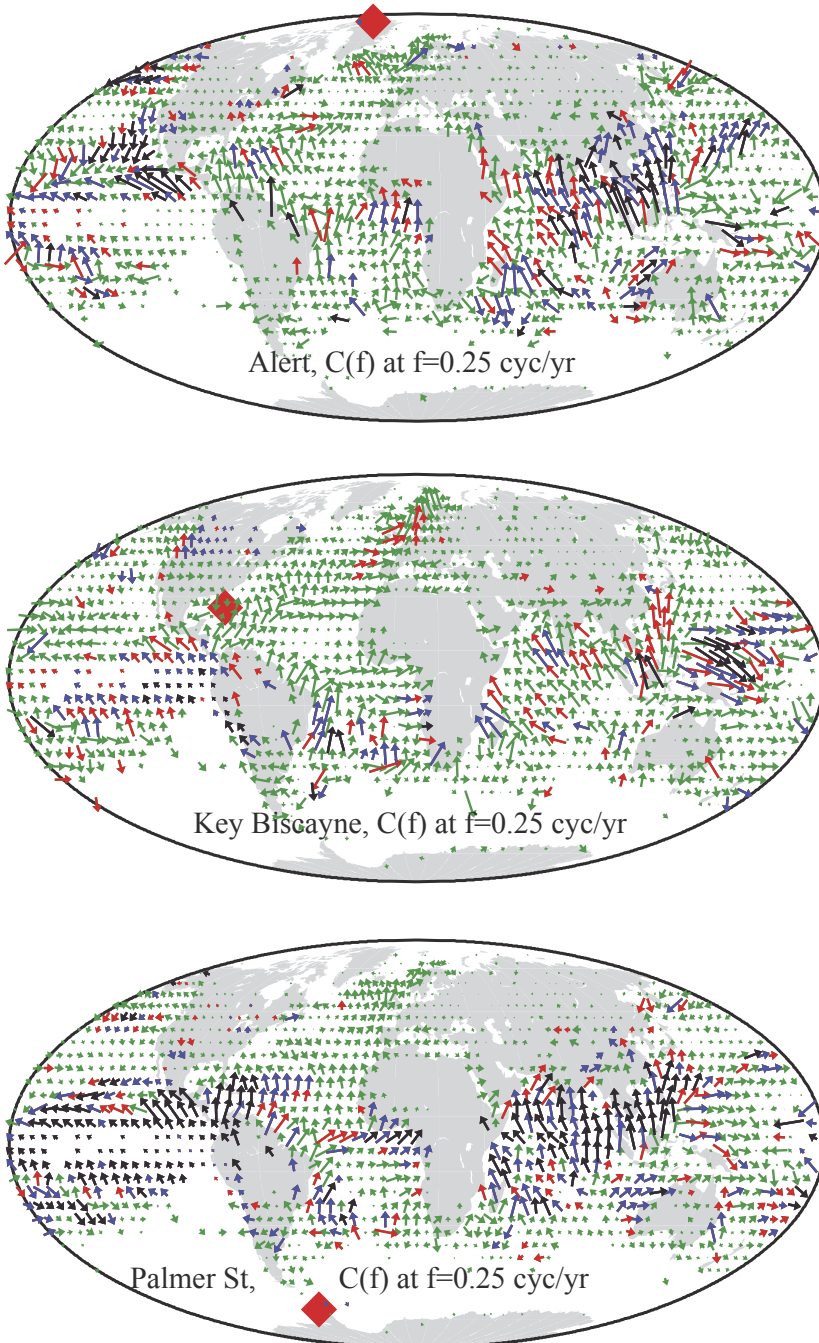


Fig. 16. Correlation transfer function between monthly gridpoint temperature anomalies (Hadley-Centre time series) and quasi-weekly CO_2 observations at GLOBALVIEW stations **alt** (Alert, Canada), **key** (Key Biscayne, Florida) and **psa** (Palmer Station, Antarctica), at ENSO bandpass $f = 0.25$ cpy for the 1979–2008 time interval. Symbol size proportional to transfer function magnitude. $|H(f)|$, with rightward arrows at 0° phase, upward arrows at 90° phase. Color-coding follows that of figure 15.

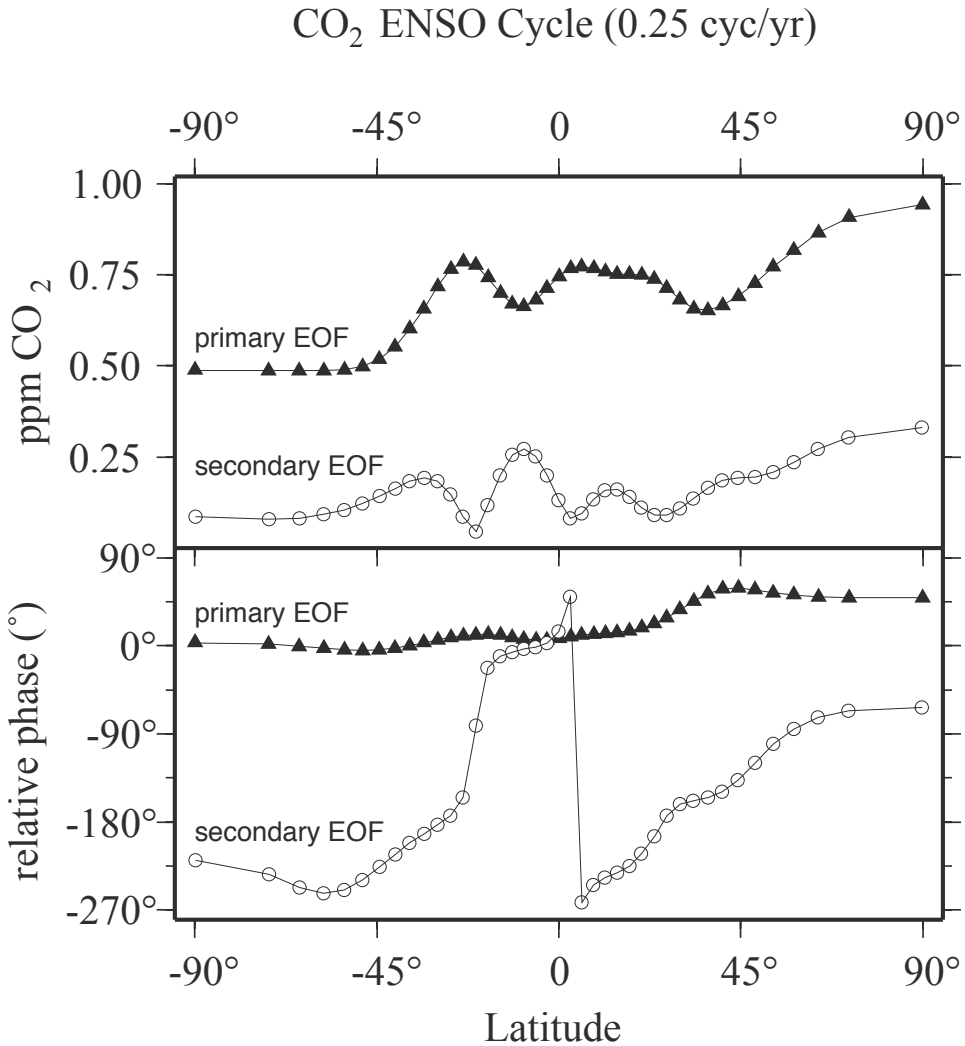


Fig. 17. Empirical orthogonal functions (EOFs) for ENSO-band CO₂ variability ($f = 0.25$ cpy) in the marine-boundary-layer (MBL) GLOBALVIEW atmospheric-CO₂ data product, which comprises 41 time series, interpolated and extrapolated from fixed-station, aircraft and ship data at evenly-spaced values of $\sin(\text{latitude})$ (GLOBALVIEW-CO₂, 2009). Upper panel graphs the amplitude of each time series in the primary and secondary EOFs versus latitude (<0 in the Southern Hemisphere). The lower panel graphs the relative phasing of the MBL time series within the EOF. The primary EOF increases amplitude in steps by a factor of two from the southern to northern polar regions, with only modest change in phase. A phase increment of $\sim 30^\circ$ occurs near 40°N latitude, corresponding to a 4-month phase lag in mid- to high-latitude Northern Hemisphere. The secondary EOF contributes a small proportion of the $f = 0.25$ cpy cycle at all latitudes.

tion, drought and fire on land (Rodenbeck and others, 2003; McPhaden and others, 2006). Tropical drought and fire have been highlighted in associating CO₂ increases with the 1997 to 1998 ENSO (Page and others, 2002). However, the largest geographical CO₂-variation in the GLOBALVIEW data set identifies the northern midlatitude continents for significant ENSO-related carbon-budget impacts. We performed a frequency-domain singular-value decomposition (SVD) on the GLOBALVIEW CO₂ marine-boundary-layer (MBL) data product to investigate global correlations. Figure 17 shows the latitude dependence of the first

two principal components at $f = 0.25$ cpy. The first principal component has 2.5 to 5 times the amplitude of the second component at all latitudes, and has only modest variation in phase, confirming the consistent behavior seen among the near continuous data series from individual stations. In low latitudes where high coherence with gridpoint temperatures is evident (fig. 15) the peak-to-peak amplitude of the signal is approximately 0.75 ppm CO₂, declining to 0.50 ppm CO₂ at high southern latitudes. This decline is crudely consistent with a signal that is generated in the tropics and transported poleward via atmospheric mixing. In the northern high latitudes, however, the principal component amplitude climbs toward 1.0 ppm CO₂, as well as exhibiting a localized increase in phase between 30°N and 45°N.

The localized phase gradient and the amplified signal argue against simple transport of tropical air toward the northern high latitudes. Despite exhibiting significant coherence with gridpoint temperature time series in low latitudes, CO₂ fluctuations north of 45°N likely are responding to a correlated extratropical climate process, that is, an ENSO teleconnection. Drought-induced fires seem unlikely, because such fires are documented mainly in tropical and southern-hemisphere land areas subject to deforestation pressure. However, mild interannual drought in the mid- to high-latitude terrestrial biosphere that effects 10 to 20 percent changes in seasonal carbon uptake could explain this signal. Apipattanavis and others (2009) found joint modes of variability between oceanic SST and the Palmer Drought Severity Index at several frequencies within the ENSO band during the 20th century at the 90 to 95 percent confidence level for nonrandomness. Figure 7B of Apipattanavis and others (2009) graphs the principal singular vector u_1 from equation (4) above. Their spectral-domain EOF at ENSO periods has substantial amplitude at gridpoints in the mid- and high-latitude Northern Hemisphere, verifying a correlation between tropical SST fluctuations and extratropical drought severity.

APPENDIX B

A FAILED HYPOTHESIS TEST FOR QUASI-ANNUAL COHERENCE

Are the local maxima in the CO₂ wavelet spectrum near $T = 1$ -yr target period (fig. 5) related to the marginal quasi-annual coherence between Mauna Loa CO₂ and global average temperature during 1958 to 1988 (figs. 2 and 3)? Close inspection suggests no. Figure 5 shows intervals of notable spectrum amplitude near 1-year period for the Mauna Loa CO₂ time series near the beginning and end of the record, but this behavior is less evident for the HadCrut3 wavelet spectrum. Some of the inverted-triangle features in the wavelet spectra resemble pulse-like signals, such as P- and S-wave arrivals in seismograms (Lilly and Park, 1995).

One of the few intervals of significant wavelet coherence near 1-yr period occurs proximal to the 1991 eruptions of the Pinatubo and Cerro Hudson volcanoes, two of the largest eruptions of the last 50 years (LeGrand and Wagenbach, 1999). The phase of the coherence near 1990 is consistent with global cooling following a rise in CO₂, the opposite of a greenhouse response, but the cause of cooling after Pinatubo is sulfate aerosols from the eruption, not its CO₂ emission (Angell, 1993; Robock, 2000). The observed CO₂ fluctuations could be due to the transient impacts of aerosols on yearly plant growth via lower temperatures (Lucht and others, 2002) or scattered-light photosynthesis (Gu and others, 2003), rather than a direct effect of volcanic CO₂ emissions. However, the wavelet spectrum of Mauna Loa CO₂ near 1-yr period peaks before the wavelet-spectrum peak in global temperatures, inconsistent with cooling causing the CO₂ fluctuation. Large eruptions during mid-century (1956 Bezymianny, 1963 Agung, 1964 Kliuchevskoi, 1975 Tolbachik) could be correlated with transient global CO₂ fluctuations near $f = 1$ cpy in figure 5, but the relative timing is inconsistent. Moreover, a lack of wavelet coherence at $f = 1$ suggests that the weakly significant coherence in annual-cycle variability in the Fourier analysis is not causally linked to a few correlated transient events.

REFERENCES

- Abramowitz, M., and Stegun, I., 1965, *Handbook of Mathematical Functions*: New York, Dover Publications, 1046 p.
- Adams, J. M., and Piovesan, G., 2005, Long series relationships between global interannual CO₂ increment and climate: Evidence for stability and change in role of the tropical and boreal-temperate zones: *Chemosphere*, v. 59, n. 11, p. 1595–1612, <http://dx.doi.org/10.1016/j.chemosphere.2005.03.0641>
- Angell, J. K., 1993, Comparison of stratospheric warming following Agung, El Chichon and Pinatubo volcanic eruptions: *Geophysical Research Letters*, v. 20, n. 8, p. 715–718, <http://dx.doi.org/10.1029/93GL00366>
- Apipattanavis, S., McCabe, G. J., Rajagopalan, B., and Gangopadhyay, S., 2009, Joint spatiotemporal variability of global sea surface temperatures and global Palmer Drought Severity Index values: *Journal of Climate*, v. 22, p. 6251–6267, <http://dx.doi.org/10.1175/2009JCLI2791.1>
- Battle, M., Bender, M. L., Tans, P. P., White, J. W. C., Ellis, J. T., Conway, T., and Francey, R. J., 2000, Global

- carbon sinks and their variability inferred from atmospheric O_2 and $\delta^{13}C$: *Science*, v. 287, n. 5462, p. 2467–2470, <http://dx.doi.org/10.1126/science.287.5462.2467>
- Bousquet, P., Peylin, P., Ciais, P., Le Quere, C., Friedlingstein, P., and Tans, P. P., 2000, Regional changes in carbon dioxide fluxes of land and oceans since 1980: *Science*, v. 290, n. 5495, p. 1342–1346, <http://dx.doi.org/10.1126/science.290.5495.1342>
- Boyce, D. G., Lewis, M. R., and Worm, B., 2010, Global phytoplankton decline over the past century: *Nature*, v. 466, p. 591–596, <http://dx.doi.org/10.1038/nature09268>
- Brohan, P., Kennedy, J. J., Harris, I., Tett, S. F. B., and Jones, P. D., 2006, Uncertainty estimates in regional and global observed temperature changes: A new data set from 1850: *Journal of Geophysical Research*, v. 111, D12106, <http://dx.doi.org/10.1029/2005JD006548>
- Buermann, W., Lintner, B. R., Koven, C. D., Angert, A., Pinzon, J. E., Tucker, C. J., and Fung, I. Y., 2007, The changing carbon cycle at Mauna Loa Observatory: Proceedings of the National Academy of Sciences of the United States of America, v. 104, n. 11, p. 4249–4254, <http://dx.doi.org/10.1073/pnas.0611224104>
- Butler, A. H., Thompson, D. W. J., and Gurney, K. R., 2007, Observed relationships between the Southern Annular Mode and atmospheric carbon dioxide: *Global Biogeochemical Cycles*, v. 21, p. GB4014, <http://dx.doi.org/10.1029/2006GB002796>
- Cadule, P., Friedlingstein, P., Bopp, L., Sitch, S., Jones, C. D., Ciais, P., Piao, S. L., and Peylin, P., 2010, Benchmarking coupled climate-carbon models against long-term atmospheric CO_2 measurements: *Global Biogeochemical Cycles*, v. 24, p. GB2016, <http://dx.doi.org/10.1029/2009GB003556>
- Canadell, J. G., Le Quere, C., Raupach, M. R., Field, C. B., Buitenhuis, E. T., Ciais, P., Conway, T. J., Gillett, N. P., Houghton, R. A., and Marland, G., 2007, Contributions to accelerating atmospheric CO_2 growth from economic activity, carbon intensity, and efficiency of natural sinks: Proceedings of the National Academy of Sciences of the United States of America, v. 104, n. 47, p. 18866–18870, <http://dx.doi.org/10.1073/pnas.0702737104>
- Chavez, F. P., Strutton, P. G., Friederich, G. E., Feely, R. A., Feldman, G. C., Foley, D. G., and McPhaden, M. J., 1999, Biological and chemical response of the equatorial Pacific Ocean to the 1997–98 El Niño: *Science*, v. 286, n. 5447, p. 2126–2131, <http://dx.doi.org/10.1126/science.286.5447.2126>
- Christy, J. R., Norris, W. B., Spencer, R. W., and Hnilo, J. J., 2007, Tropospheric temperature change since 1979 from tropical radiosonde and satellite measurements: *Journal of Geophysical Research*, v. 112, D06102, <http://dx.doi.org/10.1029/2005JD006881>
- Cleveland, W. S., and Devlin, S. J., 1980, Calendar effects in monthly time series: Detection by spectrum analysis and graphical methods: *Journal of the American Statistical Association*, v. 75, p. 487–496, <http://dx.doi.org/10.2307/2287636>
- Dettinger, M. D., and Ghil, M., 1998, Seasonal and interannual variations of atmospheric CO_2 and climate: *Tellus*, v. 50B, n. 1, p. 1–24, <http://dx.doi.org/10.1034/j.1600-0889.1998.00001.x>
- Field, R. D., van der Werf, G. R., and Shen, S. P., 2009, Human amplification of drought-induced biomass burning in Indonesia since 1960: *Nature Geoscience*, v. 2, p. 185–188, <http://dx.doi.org/10.1038/ngeo443>
- Gaillardet, J., Dupré, B., Louvat, P., and Allègre, C. J., 1999, Global silicate weathering and CO_2 consumption rates deduced from the chemistry of large rivers: *Chemical Geology*, v. 159, n. 1–4, p. 3–30, [http://dx.doi.org/10.1016/S0009-2541\(99\)00031-5](http://dx.doi.org/10.1016/S0009-2541(99)00031-5)
- GLOBALVIEW- CO_2 , 2009, Cooperative Atmospheric Data Integration Project— CO_2 , NOAA ESRL: Boulder, Colorado, <http://www.esrl.noaa.gov/gmd/ccgg/GLOBALVIEW/>
- Graham, N. E., 1994, Decadal-scale climate variability in the tropical and North Pacific during the 1970s and 1980s: observations and model results: *Climate Dynamics*, v. 10, n. 3, p. 135–162, <http://dx.doi.org/10.1007/BF00210626>
- Gruber, N., Gloor, M., Fletcher, S. E. M., Doney, S. C., Dutkiewicz, S., Follows, M. J., Gerber, M., Jacobson, A. R., Joos, F., Lindsay, K., Menemenlis, D., Mouchet, A., Muller, S. A., Sarmiento, J. L., and Takahashi, T., 2009, Oceanic sources, sinks, and transport of atmospheric CO_2 : *Global Biogeochemical Cycles*, v. 23, p. GB1005, <http://dx.doi.org/10.1029/2008GB003349>
- Gu, L., Baldocchi, D. D., Wofsy, S. C., Munger, J. W., Michalsky, J. J., Urbanski, S. P., and Boden, T. A., 2003, Response of a deciduous forest to the Mount Pinatubo eruption: Enhanced photosynthesis: *Science*, v. 299, n. 5615, p. 2035–2038, <http://dx.doi.org/10.1126/science.1078366>
- Gudasz, C., Bastviken, D., Steger, K., Premke, K., Sobek, S., and Tranvik, L. J., 2010, Temperature-controlled organic carbon mineralization in lake sediments: *Nature*, v. 466, p. 478–482, <http://dx.doi.org/10.1038/nature09186>
- Hansen, J., Ruedy, R., Glasco, J., and Sato, M., 1999, GISS analysis of surface temperature change: *Journal of Geophysical Research*, v. 104, n. D24, p. 30997–31022, <http://dx.doi.org/10.1029/1999JD900835>
- Hilley, G. E., and Porder, S., 2008, A framework for predicting global silicate weathering and CO_2 drawdown rates over geologic time-scales: Proceedings of the National Academy of Sciences of the United States of America, v. 105, p. 16855–16859, <http://dx.doi.org/10.1073/pnas.0801462105>
- Houghton, R. A., 2007, Balancing the global carbon budget: *Annual Reviews of Earth and Planetary Science*, v. 35, p. 313–347, <http://dx.doi.org/10.1146/annurev.earth.35.031306.140057>
- Hurrell, J. W., and Deser, C., 2009, North Atlantic climate variability: The role of the North Atlantic Oscillation: *Journal of Marine Systems*, v. 78, n. 1, p. 28–41, <http://dx.doi.org/10.1016/j.jmarsys.2008.11.026>
- Jones, P. D., and Briffa, K. R., 1992, Global surface air temperature variations during the twentieth century, Part 1: Spatial, temporal and seasonal details: *Holocene*, v. 2, p. 165–179.
- Keeling, R. F., 2008, Recording Earth's vital signs: *Science*, v. 319, n. 28, p. 1771–1772, <http://dx.doi.org/10.1126/science.1156761>
- Keeling, R. F., Piper, S. C., Bollenbacher, A. F., and Walker, J. S., 2009, Atmospheric CO_2 Records from Sites in the SIO Air Sampling Network: <http://cdiac.ornl.gov/trends/CO2/sio-keel.html>

- Khatiwala, S., Primeau, F., and Hall, T., 2009, Reconstruction of the history of anthropogenic CO₂ concentrations in the ocean: *Nature*, v. 462, p. 346–349, <http://dx.doi.org/10.1038/nature08526>
- Knorr, W., 2009, Is the airborne fraction of anthropogenic CO₂ emissions increasing?: *Geophysical Research Letters*, v. 36, L21710, <http://dx.doi.org/10.1029/2009GL040613>
- Koch, D., Park, J., and Del Genio, A., 2003, Clouds and sulfate are anticorrelated: A new diagnostic for global sulfur models: *Journal of Geophysical Research, Atmospheres*, v. 108, p. 4781, <http://dx.doi.org/10.1029/2003JD003621>
- Kuo, C., Lindberg, C., and Thomson, D. J., 1990, Coherence established between atmospheric carbon dioxide and global temperature: *Nature*, v. 343, p. 709–714, <http://dx.doi.org/10.1038/343709a0>
- Labitzke, K., 2005, On the solar-cycle-QBO relationship: A summary: *Journal of Atmospheric and Solar-Terrestrial Physics*, v. 67, n. 1–2, p. 45–54, <http://dx.doi.org/10.1016/j.jastp.2004.07.016>
- Lee, K., Wanninkhof, R., Takahashi, T., Doney, S. C., and Feely, R. A., 1998, Low interannual variability in recent oceanic uptake of atmospheric carbon dioxide: *Nature*, v. 396, p. 155–159, <http://dx.doi.org/10.1038/24139>
- Legrand, M., and Wagenbach, D., 1999, Impact of the Cerro Hudson and Pinatubo volcanic eruptions on the Antarctic air and snow chemistry: *Journal of Geophysical Research*, v. 104, n. D1, p. 1581–1596, <http://dx.doi.org/10.1029/1998JD100032>
- Le Quéré, C., Rödenbeck, C., Buitenhuis, E. T., Conway, T. J., Langenfelds, R., Gomez, A., Labuschagne, C., Ramonet, M., Nakazawa, T., Metzl, N., Gillett, N., and Heimann, M., 2007, Saturation of the Southern Ocean CO₂ sink due to recent climate change: *Science*, v. 316, n. 5832, p. 1735–1739, <http://dx.doi.org/10.1126/science.1136188>
- Lilly, J., and Park, J., 1995, Multiwavelet spectral and polarization analyses of seismic records: *Geophysical Journal International*, v. 122, n. 3, p. 1001–1021, <http://dx.doi.org/10.1111/j.1365-246X.1995.tb06852.x>
- Lintner, B. R., 2002, Characterizing global CO₂ interannual variability with empirical orthogonal function/principal component (EOF/PC) analysis: *Geophysical Research Letters*, v. 29, p. 1921, <http://dx.doi.org/10.1029/2001GL014419>
- Lucht, W., Prentice, I. C., Myrneni, R. B., Stith, S., Friedlingstein, P., Cramer, W., Bousquet, P., Buermann, W., and Smith, B., 2002, Climatic control of the high-latitude greening trend and Pinatubo effect: *Science*, v. 296, n. 5573, p. 1687–1689, <http://dx.doi.org/10.1126/science.1071828>
- Maasch, K. A., and Saltzman, B., 1990, A low-order dynamical model of global climatic variability over the full Pleistocene: *Journal of Geophysical Research*, v. 95, n. D2, p. 1955–1963, <http://dx.doi.org/10.1029/JD095iD02p01955>
- Mann, M. E., and Park, J., 1994, Global-scale modes of surface temperature variability on interannual to century timescales: *Journal of Geophysical Research*, v. 99, n. D12, p. 25819–25834, <http://dx.doi.org/10.1029/94JD02396>
- 1996, Joint spatiotemporal modes of surface temperature and sea-level pressure variability in the Northern Hemisphere during the last century: *Journal of Climate*, v. 9, p. 2137–2162, [http://dx.doi.org/10.1175/1520-0442\(1996\)009<2137:JSMOST>2.0.CO;2](http://dx.doi.org/10.1175/1520-0442(1996)009<2137:JSMOST>2.0.CO;2)
- 1999, Oscillatory spatiotemporal signal detection in climate studies: A multiple-taper spectral domain approach: *Advances in Geophysics*, v. 41, p. 1–131, [http://dx.doi.org/10.1016/S0065-2687\(08\)60026-6](http://dx.doi.org/10.1016/S0065-2687(08)60026-6)
- Mantua, N. J., and Hare, S. R., 2002, The Pacific decadal oscillation: *Journal of Oceanography*, v. 58, n. 1, p. 35–44, <http://dx.doi.org/10.1023/A:1015820616384>
- Martin, F., Valero, F., and Garcia-Miguel, J. A., 1994, On the response of the background atmospheric CO₂ growth rate to the anomalies of the sea-surface temperature in the equatorial Pacific ocean: *Atmospheric Environment*, v. 28, n. 3, p. 517–530, [http://dx.doi.org/10.1016/1352-2310\(94\)90128-7](http://dx.doi.org/10.1016/1352-2310(94)90128-7)
- Masarie, K. A., and Tans, P. P., 1995, Extension and integration of atmospheric carbon dioxide data into a globally consistent measurement record: *Journal of Geophysical Research*, v. 100, n. D6, p. 11593–11610, <http://dx.doi.org/10.1029/95JD00859>
- McKinley, G. A., Takahashi, T., Buitenhuis, E., Chai, F., Christian, J. R., Doney, S. C., Jiang, M.-S., Lindsay, K., Moore, J. K., Le Quéré, C., Lima, I., Murtugudde, R., Shi, L., and Wetzel, P., 2006, North Pacific carbon cycle response to climate variability on seasonal to decadal timescales: *Journal of Geophysical Research*, v. 111, p. C07S06, <http://dx.doi.org/10.1029/2005JC003173>
- McPhaden, M. J., Zebiak, S. E., and Glantz, M. H., 2006, ENSO as an integrating concept in earth science: *Science*, v. 314, n. 580, p. 1740–1745, <http://dx.doi.org/10.1126/science.1132588>
- Mears, C. A., Schnabel, M. C., and Wentz, F. J., 2003, A Reanalysis of the MSU Channel 2 Tropospheric Temperature Record: *Journal of Climate*, v. 16, p. 3650–3664, [http://dx.doi.org/10.1175/1520-0442\(2003\)016<3650:AROTMC>2.0.CO;2](http://dx.doi.org/10.1175/1520-0442(2003)016<3650:AROTMC>2.0.CO;2)
- Meehl, G. A., Hu, A., and Santer, B. D., 2009, The mid-1970s climate shift in the Pacific and the relative roles of forced versus inherent decadal variability: *Journal of Climate*, v. 22, p. 780–792, <http://dx.doi.org/10.1175/2008JCLI2552.1>
- Nagai, S., Ichii, K., and Morimoto, H., 2007, Interannual variations in vegetation activities and climate variability caused by ENSO in tropical rainforests: *International Journal of Remote Sensing*, v. 28, n. 6, p. 1285–1297, <http://dx.doi.org/10.1080/01431160600904972>
- Nevison, C. D., Mahowald, N. M., Doney, S. C., Lima, I. D., van der Werf, G. R., Randerson, J. T., Baker, D. F., Kasibhatla, P., and McKinley, G. A., 2008, Contribution of ocean, fossil fuel, land biosphere, and biomass burning carbon fluxes to seasonal and interannual variability in atmospheric CO₂: *Journal of Geophysical Research*, v. 113, p. G01010, <http://dx.doi.org/10.1029/2007JG000408>
- Obata, A., and Kitamura, Y., 2003, Interannual variability of the sea-air exchange of CO₂ from 1961 to 1998 simulated with a global ocean circulation-biogeochemistry model: *Journal of Geophysical Research—Oceans*, v. 108, 3337, <http://dx.doi.org/10.1029/2001JC001088>
- Olsen, A., Bellerby, R. G. J., Johannessen, T., Omar, A. M., and Skjelvan, I., 2003, Interannual variability in

- the wintertime air-sea flux of carbon dioxide in the northern North Atlantic, 1981–2001: Deep-Sea Research Part I, v. 50, n. 10–11, p. 1323–1338, [http://dx.doi.org/10.1016/S0967-0637\(03\)00144-4](http://dx.doi.org/10.1016/S0967-0637(03)00144-4)
- Page, S. E., Siebert, F., Rieley, J. O., Boehm, H.-D. V., Jaya, A., and Limin, S., 2002, The amount of carbon released from peat and forest fires in Indonesia during 1997: *Nature*, v. 420, p. 61–65, <http://dx.doi.org/10.1038/nature01131>
- Park, G.-H., Lee, K., Wanninkhof, R., and Feely, R. A., 2006, Empirical temperature based estimates of variability in the oceanic uptake of CO₂ over the past 2 decades: *Journal of Geophysical Research*, v. 111, p. C07S07, <http://dx.doi.org/10.1029/2005JC003090>
- Park, J., 2009, A re-evaluation of the coherence between global-average atmospheric CO₂ and temperatures at interannual time scales: *Geophysical Research Letters*, v. 36, p. L22704, <http://dx.doi.org/10.1029/2009GL040975>
- Park, J., and Levin, V., 2000, Receiver functions from multiple-taper spectral correlation estimates: *Bulletin of the Seismological Society of America*, v. 90, n. 6, p. 1507–1520, <http://dx.doi.org/10.1785/0119990122>
- Park, J., and Mann, M. E., 2000, Interannual temperature events and shifts in global temperature: A multiwavelet correlation approach: *Earth Interactions*, 4, p. 1–36, [http://dx.doi.org/10.1175/1087-3562\(2000\)004\(0001:ITEASI\)2.3.CO;2](http://dx.doi.org/10.1175/1087-3562(2000)004(0001:ITEASI)2.3.CO;2)
- Parker, R. L., 1994, *Geophysical Inverse Theory*: Princeton, New Jersey, Princeton University Press, 400 p.
- Peters, W., Jacobson, A. R., Sweeney, C., Andrews, A. E., Conway, T. J., Masarie, K., Miller, J. B., Bruhwiler, L. M. P., Pétron, G., Hirsch, A. I., Worthy, D. E. J., van der Werf, G. R., Randerson, J. T., Wennberg, P. O., Krol, M. C., and Tans, P. P., 2007, An atmospheric perspective on North American carbon dioxide exchange: CarbonTracker: Proceedings of the National Academy of Sciences of the United States of America, v. 104, n. 48, p. 18925–18930, <http://dx.doi.org/10.1073/pnas.0708986104>
- Piao, S., Ciais, P., Friedlingstein, P., Peylin, P., Reichstein, M., Luyssaert, S., Margolis, H., Fang, J., Barr, A., Chen, A., Grelle, A., Hollinger, D. Y., Laurila, T., Lindroth, A., Richardson, A. D., and Vesala, T., 2008, Net carbon dioxide losses of northern ecosystems in response to autumn warming: *Nature*, v. 451, n. 7174, p. 49–53, <http://dx.doi.org/10.1038/nature06444>
- Prieto, G. A., Parker, R. L., and Vernon, F. L., III, 2009, A Fortran-90 library for multitaper spectrum analysis: *Computers and Geosciences*, v. 35, n. 8, p. 1701–1710, <http://dx.doi.org/10.1016/j.cageo.2008.06.007>
- Qian, H., Joseph, R., and Zeng, N., 2008, Response of the terrestrial carbon cycle to the El Niño-Southern Oscillation: *Tellus Series B*, v. 60, n. 4, p. 537–550, <http://dx.doi.org/10.1111/j.1600-0889.2008.00360.x>
- Raymond, P. A., Oh, N.-H., Turner, R. E., and Broussard, W., 2008, Anthropogenically enhanced fluxes of water and carbon from the Mississippi River: *Nature*, v. 451, p. 449–452, <http://dx.doi.org/10.1038/nature06505>
- Raynaud, S., Orr, J. C., Aumont, O., Rodgers, K. B., and Yiou, P., 2006, Interannual-to-decadal variability of North Atlantic air-sea CO₂ fluxes: *Ocean Science*, v. 2, p. 43–60, <http://dx.doi.org/10.5194/os-2-43-2006>
- Reichenau, T. G., and Esser, G., 2003, Is interannual fluctuation of atmospheric CO₂ dominated by combined effects of ENSO and volcanic aerosols?: *Global Biogeochemical Cycles*, v. 17, n. 4, p. 1094, <http://dx.doi.org/10.1029/2002GB002025>
- Robock, A., 2000, Volcanic eruptions and climate: *Reviews of Geophysics*, v. 38, n. 2, p. 191–219, <http://dx.doi.org/10.1029/1998RG000054>
- Rodenbeck, C., Houweling, S., Gloor, M., and Heimann, M., 2003, CO₂ flux history 1982–2001 inferred from atmospheric data using a global inversion of atmospheric transport: *Atmospheric Chemistry and Physics*, v. 3, p. 1919–1964, <http://dx.doi.org/10.5194/acp-3-1919-2003>
- Russell, J. L., and Wallace, J. M., 2004, Annual carbon dioxide drawdown and the Northern Annular Mode: *Global Biogeochemical Cycles*, v. 18, p. GB1012, <http://dx.doi.org/10.1029/2003GB002044>
- Santer, B. D., Thorne, P. W., Haimberger, L., Taylor, K. E., Wigley, T. M. L., Lanzante, J. R., Solomon, S., Free, M., Gleckler, P. J., Jones, P. D., Karl, T. R., Klein, S. A., Mears, C., Nychka, D., Schmidt, G. A., Sherwood, S. C., and Wentz, F. J., 2008, Consistency of modelled and observed temperature trends in the tropical troposphere: *International Journal of Climatology*, v. 28, n. 13, p. 1703–1722, <http://dx.doi.org/10.1002/joc.1756>
- Schuster, U., Watson, A. J., Bates, N. R., Corbiere, A., Gonzalez-Davila, M., Metzl, N., Pierrot, D., and Santana-Casiano, M., 2009, Trends in North Atlantic sea-surface fCO₂ from 1990 to 2006: *Deep Sea Research II*, v. 56, n. 8–10, p. 620–629, <http://dx.doi.org/10.1016/j.dsr2.2008.12.001>
- Sherwood, S. C., Lanzante, J. R., and Meyer, C. L., 2005, Radiosonde Daytime Biases and Late-20th Century Warming: *Science*, v. 309, n. 5740, p. 1556–1559, <http://dx.doi.org/10.1126/science.1115640>
- Spencer, R. W., and Christy, J. R., 1990, Precise monitoring of global temperature trends from satellites: *Science*, v. 247, n. 4950, p. 1558–1562, <http://dx.doi.org/10.1126/science.247.4950.1558>
- Stallard, R. F., 1998, Terrestrial sedimentation and the carbon cycle: Coupling weathering and erosion to carbon burial: *Global Biogeochemical Cycles*, v. 12, n. 2, p. 231–257, <http://dx.doi.org/10.1029/98GB00741>
- Takahashi, T., Sutherland, S. C., Sweeney, C., Poisson, A., Metzl, N., Tilbrook, B., Bates, N., Wanninkhof, R., Feely, R. A., Sabine, C., Olafsson, J., and Nojiri, Y., 2002, Global sea-air CO₂ flux based on climatological surface ocean pCO₂ and seasonal biological and temperature effects: *Deep Sea Research Part II*, v. 49, n. 9–10, p. 1601–1622, <http://dx.doi.org/10.1016/j.dsr2.2008.12.009>
- Takahashi, T., Sutherland, S. C., Wanninkhof, R., Sweeney, C., Feely, R. A., Chipman, D. W., Hales, B., Friederich, G., Chavez, F., Sabine, C., Watson, A., Bakker, D. C. E., Schuster, U., Metzl, N., Yoshikawa-Inoue, H., Ishii, M., Midorikawa, T., Nojiri, Y., Krtzinger, A., Steinhoff, T., Hoppema, M., Olafsson, J., Arnarson, T. S., Tilbrook, B., Johannessen, T., Olsen, A., Bellerby, R., Wong, C. S., Delille, B., Bates, N. R., and de Baar, H. J. W., 2009, Climatological mean and decadal change in surface ocean pCO₂ and

- net sea-air CO₂ flux over the global oceans: Deep Sea Research Part Part II, v. 56, n. 9–10, p. 554–577, <http://dx.doi.org/10.1016/j.dsr2.2008.12.009>
- Thompson, D. W. J., Kennedy, J. J., Wallace, J. M., and Jones, P. D., 2008, A large discontinuity in the mid-twentieth century in observed global-mean surface temperature: *Nature*, v. 453, p. 646–649, <http://dx.doi.org/10.1038/nature06982>
- Thomson, D. J., 1982, Spectrum estimation and harmonic analysis: *Proceedings of the IEEE*, v. 70, n. 9, p. 1055–1096.
- 1997, Dependence of global temperatures on atmospheric CO₂ and solar irradiance: *Proceedings of the National Academy of Sciences of the United States of America*, v. 94, n. 16, p. 8370–8377, <http://dx.doi.org/10.1073/pnas.94.16.8370>
- 1990, Quadratic-inverse spectrum estimates: Applications to paleoclimatology: *Philosophical Transactions of the Royal Society of London Series A: Physical and Engineering Sciences*, v. 332, n. 1627, p. 539–597.
- Thomson, D. J., Lanzerotti, L. J., Vernon, F. L., III, Lessard, M. R., and Smith, L. T. P., 2007, Solar model structure of the engineering environment: *Proceedings of the IEEE*, v. 95, p. 1085–1132.
- Thoning, K. W., Tans, P. P., and Komhyr, W. D., 1989, Atmospheric carbon dioxide at Mauna Loa observatory 2. Analysis of the NOAA GMCC data, 1974–1985: *Journal of Geophysical Research*, v. 94, n. D6, p. 8549–8565, <http://dx.doi.org/10.1029/JD094iD06p08549>
- Trenberth, K. E., 1990, Recent observed interdecadal climate changes in the Northern Hemisphere: *Bulletin of the American Meteorological Society*, v. 71, p. 988–993, [http://dx.doi.org/10.1175/1520-0477\(1990\)071<0988:ROICCI>2.0.CO;2](http://dx.doi.org/10.1175/1520-0477(1990)071<0988:ROICCI>2.0.CO;2)
- Watson, A. J., Schuster, U., Bakker, D. C. E., Bates, N. R., Corbière, A., Gonzalez-Davila, M., Friedrich, T., Hauck, J., Heinze, C., Johannessen, T., Koertziinger, A., Metzl, N., Olafsson, J., Olsen, A., Oschlies, A., Padin, X. A., Pfeil, B., Santana-Casiano, J. M., Steinhoff, T., Telszewski, M., Rios, A. F., Wallace, D. W. R., and Wanninkhof, R., 2009, Tracking the variable North Atlantic sink for atmospheric CO₂: *Science*, v. 326, n. 5958, p. 1391–1393, <http://dx.doi.org/10.1126/science.1177394>
- Zeng, N., Mariotti, A., and Wetzel, P., 2005, Terrestrial mechanisms of interannual CO₂ variability: *Global Biogeochemical Cycles*, v. 19, p. GB1016, <http://dx.doi.org/10.1029/2004GB002273>
- Zhao, M., and Running, S. W., 2010, Drought-induced reduction in global terrestrial net primary production from 2000 through 2009: *Science*, v. 329, n. 5994, p. 940–943, <http://dx.doi.org/10.1126/science.1192666>